Dryland watersheds in flux: How nitrogen deposition and changing precipitation regimes shape nitrogen export

[1]Jianning Ren, [1]Erin J. Hanan, [2]Paolo D'Odorico, [3]Naomi Tague, [4]Joshua P. Schimel, [5]Peter M. Homyak

[1]Department of Natural Resources and Environmental Science, University of Nevada, Reno, 89501, Reno, USA

[2]Department of Environmental Science, policy, & Management, University of California, Berkeley, 94720, Berkely, USA

[3]Bren School of Environmental Science & Management, University of California, Santa Barbara, 93106, Santa Barbara, USA

[4]Department of Ecology, Evolution and Marine Biology, University of California, Santa Barbara, 93106, Santa Barbara, USA

[5]Department of Environmental Sciences, University of California, Riverside, 92521, Riverside, USA

Correspondence:

Jianning Ren (nren@unr.edu, renjianning@gmail.com)

Erin Hanan (ehanan@unr.edu)

Abstract

Atmospheric nitrogen (N) deposition and climate change are transforming the way N moves through dryland watersheds. For example, N deposition is increasing N export to streams, which may be exacerbated by changes in the magnitude, timing, and intensity of precipitation (i.e., the precipitation regime). While deposition controls the amount of N entering a watershed, the precipitation regime influences rates of internal cycling; when and where soil N, plant roots, and microbes are hydrologically connected; how quickly plants and microbes assimilate N; and rates of denitrification, runoff, and leaching. We used the ecohydrological model RHESSys to investigate (1) how N dynamics differ between N-limited and N-saturated conditions in a dryland watershed, and (2) how total precipitation and its intra-annual intermittency (i.e., the time between storms in a year), interannual intermittency (i.e., the duration of dry months across multiple years), and interannual variability (i.e., variance in the amount of precipitation among years) modify N dynamics. Streamflow N export was more sensitive to increasing intermittency and variability in N-limited vs. N-saturated model scenarios, particularly when total precipitation was lower—the opposite was true for denitrification. N export and denitrification increased or decreased the most with increasing interannual intermittency compared to other changes in precipitation amount. This suggests that under future climate change, prolonged droughts that are followed by more intense storms may pose a major threat to water quality in dryland watersheds.

Key points:

- We developed a new metric for identifying when a dryland watershed becomes "capacity N-saturated".
- Streamflow N export was more sensitive to precipitation regime changes in N-limited than N-saturated watersheds.

- N export increased or decreased the most with increasing interannual intermittency than other changes in precipitation amount.

1 Introduction

Atmospheric N deposition has been increasing in dryland watersheds of the western US since the 1860s, largely due to human population growth and concomitant increases in both fossil fuel consumption and industrial agriculture (Galloway et al., 2008; Kanakidou et al., 2016). In many populated regions around the globe, N deposition is already around 20 times higher than the natural rate of 0.05 g N g m^{-2} $year^{-1}$ (Dentener et al., 2006; Galloway et al., 2008). For example, in dryland chaparral watersheds near Los Angeles, California, the N deposition rate is more than 3 g N m^{-2} $year^{-1}$ (Benish et al., 2022). By 2050, rates are likely to reach 5 g N m^{-2} $year^{-1}$ (Sutton et al., 2007). Given these dramatic increases in N inputs, there is an urgent need to understand (1) the point at which dryland watersheds will no longer be able to assimilate additional N (i.e., the threshold of N deposition at which they become N-saturated) and (2) how deposited N will be transformed and exported from watersheds through both hydrologic and gaseous pathways (i.e., denitrification) under both N saturated and unsaturated conditions. Precipitation plays an important role in driving N cycling, uptake, and export. However, in drylands, these processes can act on different timescales and high precipitation variability can complicate our ability to predict the fate of atmospherically deposited N (Homyak et al., 2014; Howarth et al., 2006; Krichels et al., 2022; Ren et al., 2023, submitted).

Conceptual models used to assess N saturation and N export were developed in temperate systems where relatively high and consistent rainfall maintains hydrologically connected soils throughout the year, allowing substrates to diffuse to plant roots and be taken up (Homyak et al., 2014). As a result, these models assume that N export occurs once a watershed exceeds the

capacity of plants and other ecosystem components to assimilate N and becomes N-saturated (Aber et al., 1989). In drylands however, summer aridity can keep soils dry for months without rain, limiting subsurface N transport and allowing it to accumulate in hydrologically disconnected microsites (i.e., hotspots; Parker & Schimel, 2011). At the onset of the wet season when rains return, N can be rapidly exported before plants and soil microbes can assimilate it—this can produce large stream N losses (known as "pulses") that under traditional conceptual models would suggest N saturation (Zhu et al., 2018). However, such hydrologic losses regularly occur in drylands even when plants remain N-limited (Homyak et al., 2014).

To better account for asynchronies between N availability and uptake, Lovett & Goodale. (2011) introduced the concept of **kinetic** N saturation, where available N can exceed demand over short timescales (e.g., when a storm follows a long dry period). This contrasts with **capacity** N-saturation, where an ecosystem or watershed can no longer assimilate N over longer timescales, resulting in consistent increases in N export that correspond with increasing atmospheric N inputs. Because both N saturation statuses can increase N export, it is difficult to identify the threshold at which dryland watersheds shift from kinetic to capacity saturation. As a result, it also remains difficult to predict the fate of atmospherically deposited N and how it changes along a gradient from kinetic to capacity saturation.

Further complicating our understanding of N saturation and export, general circulation models project changes in the both the total amount and timing of precipitation in drylands (Fischer et al., 2013). These changes can occur on both intra- and interannual scales (Knapp et al., 2002; Trenberth et al., 2003). On intra-annual time scales, a higher water-holding capacity in a warming atmosphere can give rise to larger precipitation events with longer dry periods between storms (i.e., higher *intra-annual intermittency*, Allen & Ingram, 2002). At interannual

scales, climate change can alter atmospheric circulation and moisture transport to promote extreme wet months with a longer duration of dry months across multiple years (i.e., higher *interannual intermittency* (Allen & Ingram, 2002; Trenberth et al., 2003). Alternatively, some models project that climate change will enhance *interannual variability*, making dry years drier and wet years wetter, while still retaining the intra-annual storm event characteristics (Pörtner et al., 2022). Higher precipitation intermittency and variability can both affect N export, but increases in intermittency, which change both the timing and magnitude of storms (i.e., fewer, more intense storms), may have a different effect than changes in variability alone (which only influences storm size without changing timing (Homyak et al., 2017; Winter et al., 2023). Recent studies have shown that enhanced precipitation variability and intermittency can increase both nitric oxide (NO) emissions and stream N export (Krichels et al., 2022; Winter et al., 2023), however, most of these studies are event-based and the long-term, and cumulative effects of altered precipitation regimes and their interactions with N deposition remain poorly understood.

A simulation modeling approach should be useful for identifying the threshold of atmospheric N deposition at which a watershed transitions from kinetic to capacity saturation, which would enable us to better project future N export. With this approach, we can directly investigate how N export responds to temporal asynchrony between N availability and uptake; for example, when the first rain event of a wet season flushes N while plants are not actively growing (in a Mediterranean climate) vs. when the activation of rainy season overlaps with the peak growing season in early spring (in a continental climate). We expect that when a watershed only experiences kinetic saturation, there will be pronounced differences between these two scenarios. Conversely, when a watershed is capacity N-saturated due to high N-deposition, total N export will not change in response to the timing of precipitation.

Using a simulation modeling approach, we developed and tested our proposed metric for identifying when a dryland watershed becomes "capacity N-saturated." Then using the new metric, we developed N-limited and N-saturated scenarios to address two questions: (1) How do changes in the precipitation regime, including the total amount of precipitation, its intra-annual intermittency, interannual intermittency, and interannual variability influence watershed-scale N export, and (2) How do these responses differ between N-limited and N-saturated watersheds? These scenarios were conducted using the coupled ecohydrological-biogeochemical model RHESSys (Tague & Band, 2004) in a dryland, chaparral-dominated watershed downwind of Los Angeles, California that experiences high rates of N-deposition.

2 Methods

2.1 Study site

We developed modeling scenarios for the chaparral-dominated Bell 4 watershed in the San Dimas Experimental Forest, located 50 km northeast of Los Angeles, California (34°12′N, 117°47′W). This is a small watershed (0.14 km^2) with elevations ranging from 700 to 1024 meters. The soils are shallow, coarse-textured sandy loams weathered from granitic parent material (Chaney et al., 2016; Dunn et al., 1988); they classify as Typic or Lithic Xerorthents (Hubbert et al., 2006; Ryan, 1991). The climate is characterized by hot and dry summers and cool-humid winters. Mean annual precipitation is approximately 700 mm, with daily temperatures ranging from -8°C in winter to 40 °C in summer. Vegetation on south-facing slopes includes chamise (*Adenostoma fasciculatum*), California lilac (*Ceanothus spp*.), and black sage (*Salvia mellifera*), while north-facing slopes are covered by *ceanothus spp.* and California laurel (*Umbellularia californica)*. Riparian areas are dominated by live oak (*Quercus agrifolia*). Being

downwind from a major metropolitan area, Bell 4 experiences high N deposition rates, which exceed 30 kg ha^{-1} $year^{-1}$ (Benish et al., 2022; Bytnerowicz & Fenn, 1996).

2.2 RHESSys model

To investigate how precipitation regime changes affect N cycling and export in drylands and how they are different between N-limited and N-saturated watersheds, we used the regional hydro-ecologic simulation system (RHESSys). RHESSys is a spatially distributed model that fully couples hydrological processes with biogeochemical processes, allowing it to simulate the effects of climate and environmental change on C and N cycling and hydrologic conditions (Garcia et al., 2016; Lin et al., 2015; Tague & Band, 2004). Recent model improvements have enabled RHESSys to better-represent N cycling and transport in dryland watersheds (Burke et al., 2021; Hanan et al., 2017, Ren et al., 2023, submitted). This includes refining nitrification processes after wildfire in chaparral (Hanan et al., 2017), and representing biogeochemical hotspots explicitly across a landscape (Ren et al., 2023, submitted). RHESSys has been extensively evaluated in several dryland watersheds across the western US (Burke et al., 2021; Chen et al., 2020; E. S. Garcia & Tague, 2015; Elizabeth S. Garcia et al., 2016; Hanan et al., 2017, 2021; Ren et al., 2021, 2022; Reyes et al., 2017; Stephens et al., 2022).

C and N cycling among vegetation, litter, and soil layers are simulated at a patch scale (the smallest spatial unit; 3-meter resolution in this study). Photosynthesis is calculated using the Farquhar model which is a function of stomatal conductance, radiation, nitrogen and carbon dioxide concentration, air temperature and atmospheric pressure (Farquhar & von Caemmerer, 1982). Plant respiration includes maintenance and growth respiration, which is estimated using Ryan. (1991) model. Carbon is then allocated to roots, stems, and leaves using an architecture (or age) based method (Dickinson et al., 1998). RHESSys has four litter pools and four soil pools

158 with different C:N ratios and decomposition rates. Decomposition is estimated based on a
159 defined maximum decomposition rate and constrained by soil moisture, soil temperature, and
160 nitrogen availability. N mineralization and immobilization are estimated using the C:N ratios of
161 the litter and soil pools when materials decompose from one pool to another (Hanan et al., 2017;
162 Tague & Band, 2004).

163 RHESSys calculates nitrification rates based on the $CENTURY_{NGAS}$ model which is a
164 function of soil pH, soil moisture, soil temperature, and available soil ammonium (Parton, 1996).
165 A maximum denitrification rate is calculated as a function of the total available nitrate (NO_3^-) in
166 soil, and total soil carbon and nitrogen, and then the maximum rate is modified based on soil
167 moisture and soil respiration as a proxy for microbial abundance.

168 Soil moisture processes include four vertical layers, a surface detention store, a root zone
169 store, an unsaturated store, and a saturated store. At a daily timestep, the surface detention store
170 receives water from canopy throughfall and snowmelt (when present), and infiltrates into the soil
171 based on the Phillip (1957) infiltration equation. Overland flow is generated when the ponded
172 water is above the detention storage capacity. Water can percolate into a deeper ground water
173 store through bypass flow. Water drains from the unsaturated zone or root zone to the saturated
174 zone based on hydraulic conductivity and moves from the saturated zone to the unsaturated zone
175 or root zone based on the Eagleson (1978) equation. Subsurface lateral flow between patches
176 follows topographic gradients and soil hydraulic parameters such as saturation deficit and
177 transmissivity. N moves with these water fluxes based on its concentration (Tague & Band,
178 2004). Atmospherically deposited N enters the soil through infiltration from the surface
179 detention store. In the unsaturated zone, soil nitrate decreases exponentially with depth. In the

saturated zone, nitrate export follows a flushing hypothesis, where more soil N becomes available for flushing to streams as the water table rises (Chen et al., 2020).

To account for sub-grid scale heterogeneity in vegetation cover, RHESSys can be run using a new aspatial framework (Burke et al., 2021). In this new framework, "patch families" are the smallest spatially explicit model unit, and "aspatial patches" nested within a patch family are the smallest aspatial model unit. Aspatial patches do not have physical locations, but instead represent a distribution of vegetation types based on observed or hypothetical distributions. Local routing of water between aspatial patches within a patch family is based on the relative moisture differences among aspatial patches in the rooting and unsaturated zones and mediated by user-defined gaining and losing coefficients for each patch type (Burke et al., 2021). Local routing in the saturated zone is based on the differences in the groundwater table and it carries nitrate when exchanging water.

We also recently expanded the aspatial patch framework to incorporate the role of fine-scale biogeochemical "hotspots," represented as aspatial patches within each patch family—these represent a distribution of microsites (e.g., soil aggregates) where biogeochemical cycling can be hydrologically disconnected, as soils dry out, from other aspatial patches that contain plant roots (Ren et al. 2023, submitted). Hotspots help drive kinetic N saturation by enabling N to accumulate and subsequently be flushed from the system when soils are rewetted.-To model hotspot dynamics, the framework includes: (1) model algorithms that enable hotspots to access soil and litter C and N from neighboring non-hotspot patches for decomposition and biogeochemical cycling, and (2) algorithms and parameters that control the moisture conditions under which hotspots are hydrologically disconnected from other aspatial patches in the saturated zone, (3) parameters that control water diffusion in the unsaturated and/or root zone between

hotspot and non-hotspot patches as soils dry out. For detailed descriptions of the RHESSys model and the new hotspot framework, refer to Tague & Band, (2004) and Ren. et al (2023, under review).

2.3 Data

To represent topography across the watershed, we used a 1-meter resolution digital elevation model (DEM) from LiDAR aggregated to 10-meters (Ren et al., 2023, submitted). Soil texture was delineated across the watershed using the POLARIS database (Chaney et al., 2016). To map landcover across Bell 4, we aggregated 1-meter resolution land cover data from the National Agriculture Imagery Program (NAIP; collected on June 5, 2016) to 3-meters. We then classified three land cover types across the watershed: chaparral, live oak, and bare ground (Maxwell et al., 2017). RHESSys patch families were established based on the 10-meter DEM, while the aspatial patch vegetation distributions were classified based on the 3-meter NAIP data (Ren et al., 2023, submitted). The Bell 4 basin contained 1259 patch families, with each patch family having approximately 11 aspatial patches. We acquired meteorological forcing data from 1979 to 2020 from the gridMET, including daily maximum and minimum temperatures, precipitation, relative humidity, radiation, and wind speed (Abatzoglou, 2013). Daily streamflow data from 1980 to 2002 and stream N data from 1988 to 2000 were provided by U.S. Forest Service (USFS).

2.4 Model initialization and calibration

To initialize soil C and N pools to steady state, we spun RHESSys up for three hundred years. Then to initialize vegetation C and N pools, we used a target-driven spin-up approach, which leverages remotely sensed LAI calculated from NAIP (at April 24, 2010) to set target values for each patch across the watershed; this enables us to spin the model up mechanistically

while still capturing landscape heterogeneity (Hanan et al., 2018). We then calibrated six soil parameters using observed streamflow data: saturated hydraulic conductivity (K_{sat}), the decay of K_{sat} with depth (m), pore size index (b), air entry pressure (ϕ), bypass flow to deeper groundwater storage (gw_1), and deep groundwater drainage rates to stream (gw_2). We selected the best parameters by comparing the observed and modeled streamflow using the monthly Nash-Sutcliffe efficiency (NSE; Nash & Sutcliffe, 1970) and percent error of annual streamflow. We used eight years of streamflow data from 1993 to 2002 for calibration and three years from 1980 to 1983 for validation. Following calibration, we designated one aspatial patch in each patch family to represent hotspots, assuming that hotspots were evenly distributed across the landscape. We then optimized the hotspot-related parameters (i.e., the water sharing coefficient between aspatial patches and subsurface flow threshold) by comparing modeled and observed streamflow N from 1988 to 2000. During the calibration, the monthly NSE of simulated streamflow reached 0.88 with a percent error of 5.45%, while for the validation period, the monthly NSE was 0.80 with a percent error of -3.92%. This suggests a close match between modeled and measured streamflow timing and volume. By including hotspots in the model, we also improved our ability to capture the timing of peak streamflow nitrate observations (NSE = 0.40). A more detailed description of initialization and calibration results can be found in Ren et al. (2023, submitted).

2.4 Scenarios

2.4.1 Developing better metrics for N-saturation in dryland watersheds.

Because seasonal N export to streams is characteristic in dryland watersheds, even when they are not N-polluted (Homyak et al., 2014), we need to develop metrics that can identify when a watershed shifts from kinetic to capacity saturation (Lovett & Goodale, 2011). This requires

understanding how N deposition interacts with the timing of precipitation. To determine the N deposition threshold at which a watershed becomes N-saturated, we built scenarios considering interactions between the N deposition rate and precipitation seasonality over a period of 60 years. Because the observed meteorological forcing data spans only 40 years (water years 1980 to 2020), we repeated this data to construct the additional 20 years. This included three scenarios for precipitation seasonality: a dry summer scenario (to match observations), a wet summer scenario (to represent a more continental climate), and an evenly distributed scenario (Figure 1a). The wet summer and evenly distributed scenarios were reconstructed from the observed precipitation data by manipulating the duration of dry days and the timing of precipitation using a method from Rodriguez-Iturbe et al. (1999) which will be introduced in detail in section 2.4.2. We also included 12 dry N deposition scenarios (including 0.05, 0.25, and 0.5 to 5 g m^{-2} $year^{-1}$ at an increment of 0.5 g m^{-2} $year^{-1}$). This resulted in 36 scenarios for precipitation and N deposition in a factorial design.

To determine the level of N deposition at which our watershed becomes N-saturated, we examined N export for each scenario and determined the magnitude of N deposition where export no longer varied under different precipitation seasonality scenarios. This approach assumes that under kinetic saturation, dry summers would promote more N export because rainfall occurs when plants are less active. We define the N deposition threshold above which the watershed is capacity N saturated as the amount of N deposition required for mean normalized streamflow N (i.e., annual streamflow N divided by the N deposition rate) in both the dry summer and the evenly distributed scenarios to be above 90% of the mean normalized streamflow in the dry winter scenario. Using this threshold, we then built two scenarios for N saturation status: N-saturated and N-limited. This involved scaling N deposition up or down such

that the N saturated scenario had 100 times higher N deposition than the N-limited scenario. We then used these scenarios for the following sensitivity analysis to examine how precipitation intermittency and variability influence N export under saturated and unsaturated conditions.

2.4.2 Effects of intra-annual precipitation intermittency on N export

To understand the how intra-annual precipitation intermittency influence N export, we used a stochastic precipitation generator, based on Rodriguez-Iturbe et al. (1999). Within a given year, the occurrence and amount of total daily precipitation can be viewed as a stochastic process. Specifically, the occurrence of rainfall is modeled as a **Poisson process with a rate λ (average rainfall frequency)**, and the amount of rainfall for each event is determined by a random exponential distribution. As our model operates on a daily timestep, we did not consider the temporal structure of rainfall within each event and instead assumed the precipitation occurred instantaneously.

Based on these assumptions, the distribution of the length of dry days (τ) between precipitation events is an exponential distribution with a mean 1/ λ (the unit of λ is 1/day).

$$f_\tau(\tau) = \lambda e^{-\lambda\tau},\ for\ \tau \geq 0 \qquad \text{Eq (1)}$$

The amount of precipitation is an independent random variable *h (mm/day)*, calculated by an exponential probability density function:

$$f_H(h) = \frac{1}{\alpha} e^{-\frac{h}{\alpha}},\ for\ h \geq 0 \qquad \text{Eq (2)}$$

Where α is the mean of daily rainfall amount (mm/day) when precipitation occurs for a certain year and can be estimated from the observed data.

The total amount of precipitation R (mm year^{-1}) for a given year can therefore be calculated as

$$R = h \times T/\tau \quad \text{Eq (3)}$$

Where T is the total days for a rainy season.

We estimated the two parameters (λ_0 and α) for the stochastic model based on observed precipitation. Then we adjusted the rainfall frequency parameter 1/λ_0 by a factor of 2 to 4 to increase the duration of dry days between rainfall events. Additionally, we adjusted the mean daily rainfall amount α to maintain consistent total precipitation amounts across different scenarios. In total, we developed five distinct intra-annual intermittency scenarios (Figure 1b).

To summarize, within one year, this method determines the number of dry days across a rainy season and uses rainfall intensity and the number of days with precipitation (from observations) to determine the size and timing of storms that occur between dry days. This enables us to vary rainfall intermittency, while maintaining a fixed amount of precipitation for each year. Then, to examine how precipitation intermittency interacts with the total amount of precipitation (e.g., under drier vs. wetter futures), we developed five precipitation scalers for each intermittency scenario (ranging from 0.6 to 1.4 at an increment of 0.2). Hereafter, we refer to scenarios with precipitation scaling factors less than one as "drier future" scenarios and greater than one as "wetter future" scenarios. By combing five precipitation scaling factor scenarios, two N saturation scenarios, and five intra-annual intermittency scenarios, we generated a total of 40 different scenarios in a factorial design and ran the model for 60 years (Figure 2).

2.4.3 The effect of interannual intermittency on N export

To investigate the effects of interannual precipitation intermittency on N export, we used a stochastic precipitation generator that was similar to the one used for the intra-annual precipitation intermittency analysis. Specifically, we examined monthly precipitation data for a

315 period of 40 years (in total 480 months) and modeled both the amount of monthly precipitation
316 and duration of dry months as stochastic processes. We initially ignored the temporal structure of
317 precipitation within each month and calculated the two parameters λ_0 (unit is 1/month) and α
318 (mm/month). We then downscaled the modeled monthly precipitation to a daily timestep based
319 on observed precipitation considering the temporal structure of rainfall events within a month.
320 To increase the interannual intermittency, we then manipulate the two parameters (λ and α) to
321 increase both the duration and the mean amount of monthly precipitation while maintaining
322 consistent total precipitation levels over the 40-year period (Figure 1d). Again, we built 40
323 scenarios by combining the five interannual intermittency scenarios with the previous four
324 precipitation scaling factors and the two N saturation scenarios and ran RHESSys for 60 years by
325 looping the 40 years reconstructed data.

326 2.4.4 Effect of interannual precipitation variability on N export

327 To understand the effects of interannual precipitation variability on N export, we adapted
328 methodology proposed by Gherardi & Sala (2015). We generated different scenarios for
329 interannual precipitation variability by manipulating the observed precipitation data. To increase
330 variability, we increased the annual precipitation amount in wet years and decreased it in dry
331 years (by 20%, 40%, 60% relative to the observed amounts). To decrease variability, we lessened
332 the amount of annual precipitation in wet years and increased it in dry years (by 20%, 40%, 60%
333 and 80%). This approach enabled us to create scenarios with varying coefficients of variation
334 (CV) while keeping the total precipitation the same throughout the simulation period. This
335 resulted in eight interannual variability scenarios including a baseline scenario (Figure 1c). By
336 combing them with five total precipitation scaling factors, and two levels of N saturation (N-
337 limited vs. N-saturated), we generated 80 factorial scenarios.

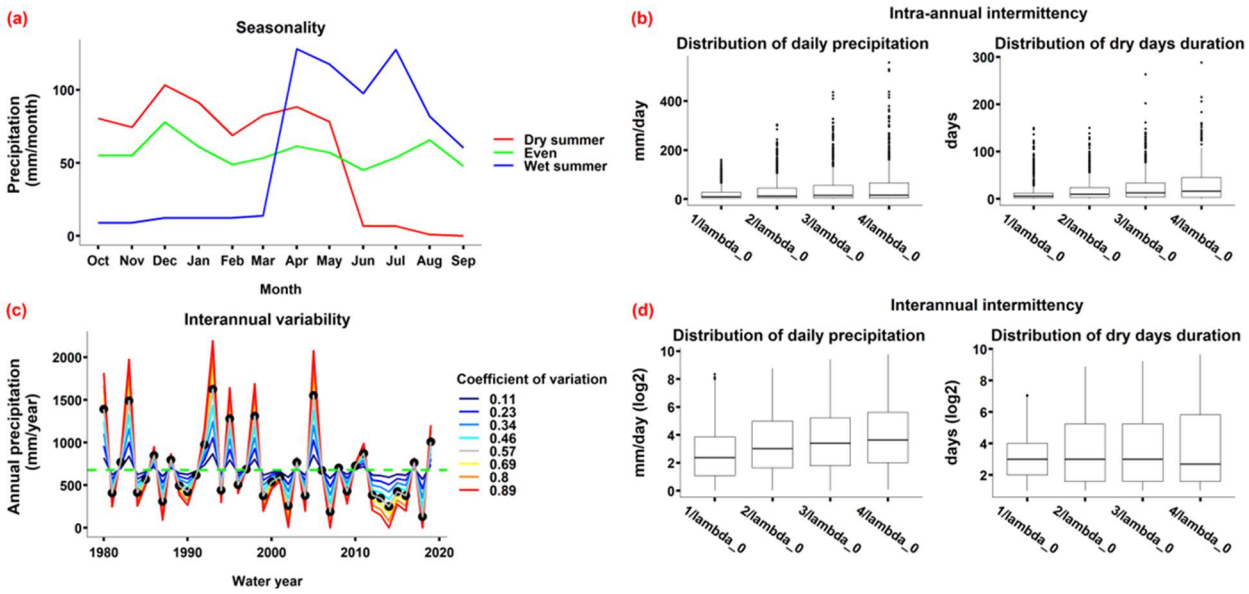

Figure 1. A summary of reconstructed precipitation data used. Panel a represents the precipitation seasonality scenarios: dry summer, evenly distributed across the year, and wet summer. The dry summer scenarios used observed precipitation data. Total precipitation and inter-annual intermittency over the 40 years was consistent across three scenarios. Panel b represents the reconstructed precipitation data with different intra-annual intermittencies for a period of 40 years, including the distribution of daily precipitation and dry days duration. The total amount of precipitation over 40 years was the same for all four precipitation intermittency scenarios. Lambda (λ_0) is the frequency of observed rain events, and the x-axis shows an increase in intermittency. The comparison between observed and reconstructed precipitation of $1/\lambda_0$ is shown in Figure S1. Panel c represents reconstructed and observed precipitation for different levels of interannual variability. The green horizontal line is the mean annual precipitation from the observation data and the black dots are the observed annual precipitation. Blue lines correspond with lower variability relative to observation, red lines correspond with higher variability relative to observation. Panel d represents reconstructed precipitation data with different interannual intermittencies for a period of 40 years, including the distribution of daily precipitation amounts and the distribution of duration of dry days. The total amount of precipitation over 40 years was the same for all five precipitation scenarios at a given precipitation scaling factor. Lambda (λ_0) is the frequency of reconstructed baseline rain events, and the x-axis shows an increase in intermittency. Note that the y axis is in $\log_2$ scale to better show extreme values.

To summarize, we developed two scenarios for N saturation status (N-saturated vs N-limited), five precipitation scaling factors (0.6, 0.8, 1, 1.2, 1.4), and three sets of scenarios for changes in precipitation timing. These changes include four intra-annual intermittency scenarios, four interannual intermittency scenarios, and eight interannual variability scenarios. This resulted

in 160 factorial scenarios (Figure 2). We then calculated the normalized differences in N fluxes for each precipitation regime relative to its baseline, defined as the lowest variability or intermittency scenario for each precipitation scaling factor and N saturation status. For example, in the N-limited scenarios, to compare N export among intra-annual intermittency scenarios at a given precipitation scaling factor, we calculated differences between a given intermittency scenario and the baseline ($1/\lambda\_0$). This resulted in 5 baseline intermittency scenarios (two drier, two wetter, and a scenario with the baseline precipitation variability and total amount). The combination of high precipitation scaling factors and high intermittency/variability can interact to create some extreme storms that are historically unprecedented, though within the range of possible future projections (Knapp et al., 2015). However, median storm sizes are well within the range of historical variability for these semiarid systems; we focus on median values in our discussion.

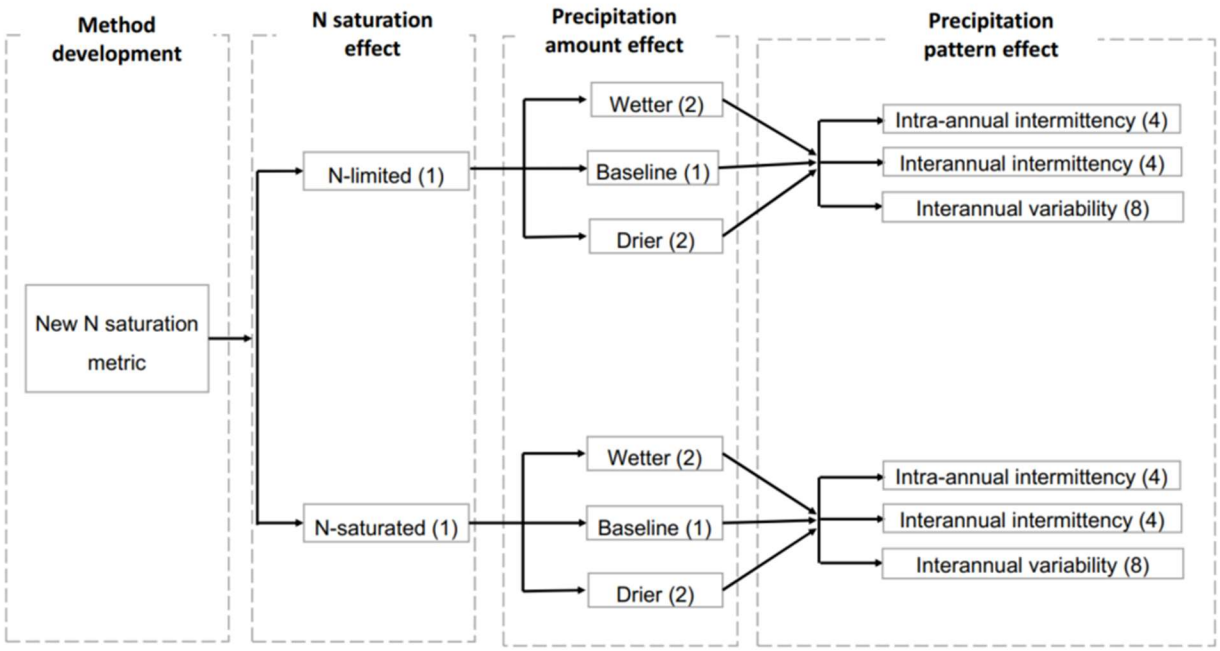

Figure 2. Summary of the scenarios developed to examine how interactions between N deposition and changes in precipitation regime affect N export. The number inside the parenthesis indicates the number of corresponding scenarios.

3 Results

3.1 A better metric for N saturation in drylands

In scenarios with relatively low atmospheric N deposition (i.e., smaller than 1 g m^{-2} $year^{-1}$), the mean and distribution of annual streamflow N (over 60 years) varied depending on the seasonality of precipitation, with the dry summer scenario resulting in the highest export and the wet summer scenario resulting in the lowest (Figure 3 and Figure S2). However, as N deposition increased, the watershed became less N-limited, leading to similar mean values and streamflow N distributions across different precipitation seasonality scenarios. This can be attributed to the fact that in a watershed with dry summers, the wet winter period can flush N to streams before plants begin to take it up, whereas in watersheds with wet summers, N is consumed by plants prior to leaching, resulting in less streamflow N export. Consequently, it can be inferred that

when the watershed is N-limited, the dry summer scenario would yield higher streamflow N export than the dry winter scenario. Conversely, in an N-saturated watershed, the consumption of N by plants and microbes would have a much smaller effect on streamflow N export. Using this logic, we identify an N deposition threshold of approximately 2 g m^{-2} $year^{-1}$ above which the watershed becomes N-saturated. At this threshold, the ratio of the normalized mean annual streamflow N for the wet summer:dry summer scenarios was no smaller than 0.9 (the same was true for the evenly distributed scenario; Figure 3). For the following scenarios, we selected 0.05 g m^{-2} $year^{-1}$ and 5 g m^{-2} $year^{-1}$ to represent extremes of N-limited and N-saturated systems, respectively.

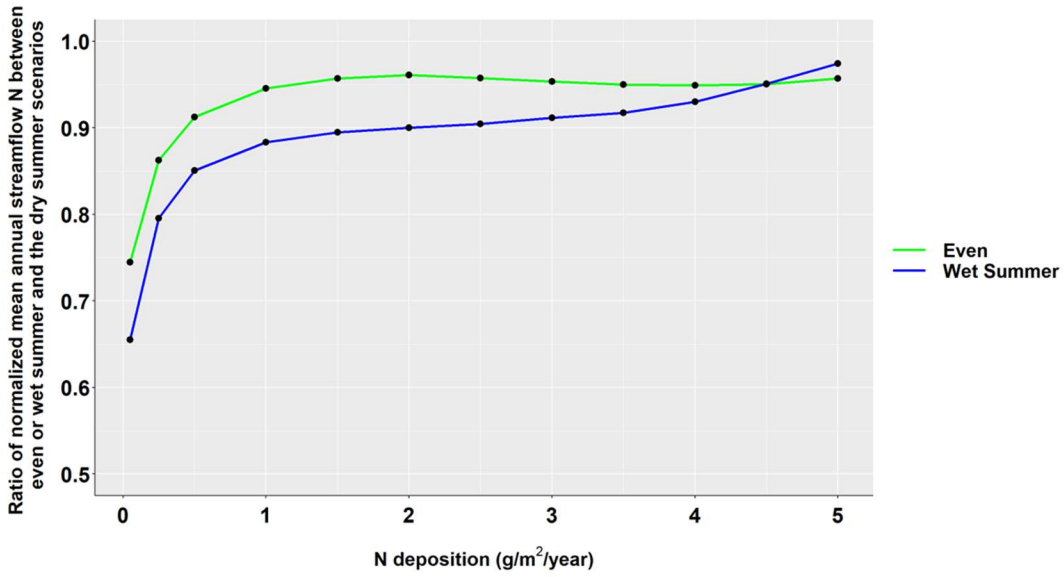

Figure 3. Ratio of the normalized mean annual streamflow N export between scenarios (calculated as wet summer/dry summer (blue line) or even/dry summer (green line); values are normalized by the N deposition rate). We selected an N saturated threshold where normalized streamflow N in the wet summer scenario was no smaller than 90% of that observed in the dry summer scenario. We used mean, rather than median values to account for extreme values.

3.2 The effect of changing precipitation regimes on N export.

3.2.1 The effect of intra-annual precipitation intermittency on N export.

Streamflow N export increased with higher intra-annual intermittency, which alters both the timing and magnitude of storms (Figure 4). Moreover, in N-limited scenarios, a higher total precipitation scaling factor generally increased streamflow N export (Figure 4). However, in N-saturated scenarios, baseline conditions can lead to more streamflow N export (Figure 4a). Higher intermittency implies longer dry periods and greater differences in precipitation amount between dry and wet periods, despite the same total precipitation among scenarios over the 60-year simulation. This can increase soil N accumulation during dry periods while reducing denitrification and N uptake (model estimates of plant carbon declined from 6 kg m^{-2} to around 4 kg m^{-2} between the highest and lowest intermittency scenario, Figure S4b). As a result, more N is flushed to streams during the wet periods. For both N-limited and N-saturated scenarios, denitrification decreased with higher levels of intermittency (Figure 4 b and e), primarily due to slower rates of decomposition caused by decreases in plant growth and litter production (Figure S4a).

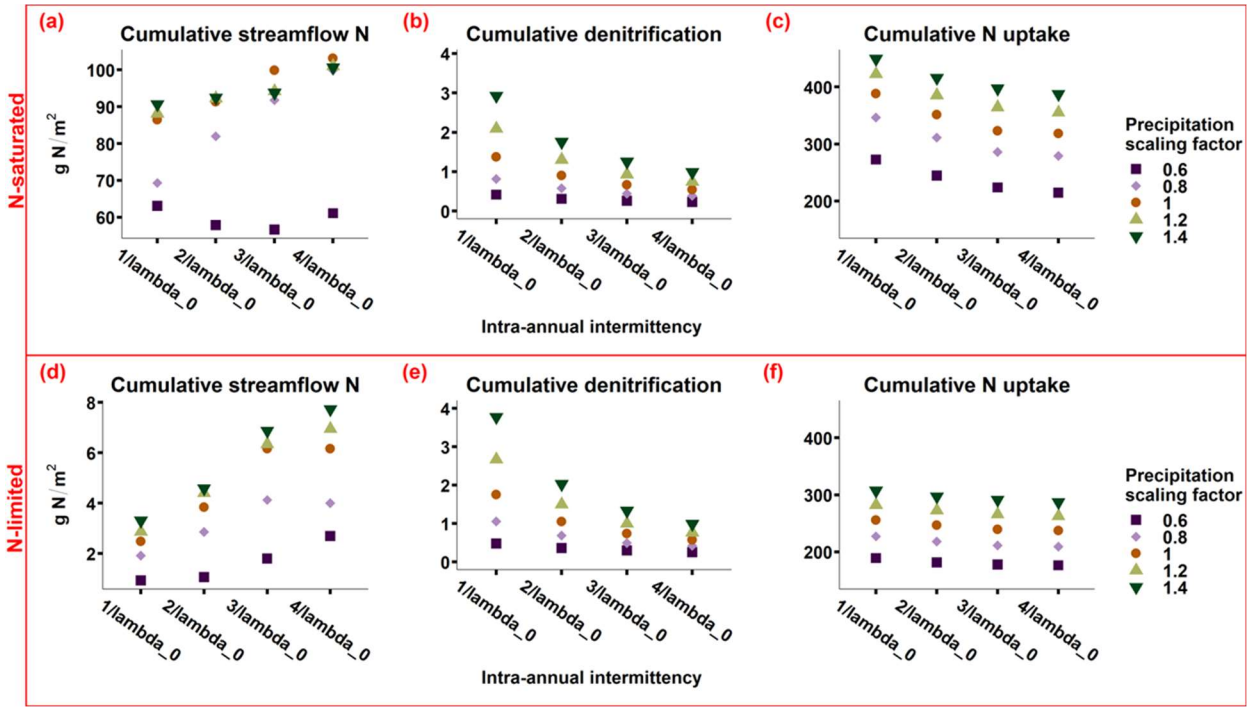

Figure 4. Sensitivity of cumulative N fluxes over 60 years (absolute value) to intra-annual precipitation intermittency for N-saturated and N-limited scenarios. The x axis is the duration of dry days between rainfall event, larger values represent higher intra-annual intermittencies.

Streamflow N export and denitrification were more sensitive to intra-annual precipitation intermittency in N-limited scenarios than in N-saturated scenarios, while plant N uptake was more sensitive to intra-annual intermittency in N saturated scenarios (Figure 5). For example, plant C declined 12% (from 3.9 to 3.4 kg m^{-2}) in N-limited scenarios but declined 27.5% (from 5.8 to 4.2 kg m^{-2}) in N-saturated ones (Figure S4a). The declines in plant carbon with higher intra-annual intermittency were smaller in N-limited scenarios because plants can be limited by both N and water, and changing water availability does not matter as much in N-limited as it does in N saturated scenarios, where once N limitation was alleviated, vegetation growth became more limited by water availability. In addition, streamflow N export increased with higher levels of intra-annual intermittency, while denitrification decreased (Figure 5a, b). This suggests

increases in intra-annual intermittency can increase N export to streams while decreasing N losses to the atmosphere.

In N-saturated scenarios, streamflow N export was most sensitive to variation in intra-annual intermittency under a precipitation scaling factor of 0.8, while in N-limited scenarios, scaling factors of 0.6 or 1 were the most sensitive (Figure 5a, b). In N-limited scenarios, the 0.6 scaling factor showed the strongest exponential increases in streamflow N export with increasing intermittency, indicating that the drier future scenarios have the largest sensitivity to intermittency changes.

Denitrification in the wetter future scenarios decreased more with increasing intra-annual precipitation variability than in the drier future scenarios because total denitrification was higher in wetter baseline intermittency scenarios ($1/\lambda\_0$). With greater intra-annual intermittency, these decreases were larger (Figure 5b, e). By contrast, in dry scenarios, plant N uptake decreased slightly more with increasing intra-annual intermittency than in wetter scenarios, but the magnitude was relatively small compared to streamflow N export and denitrification ((Figure 5c, f).

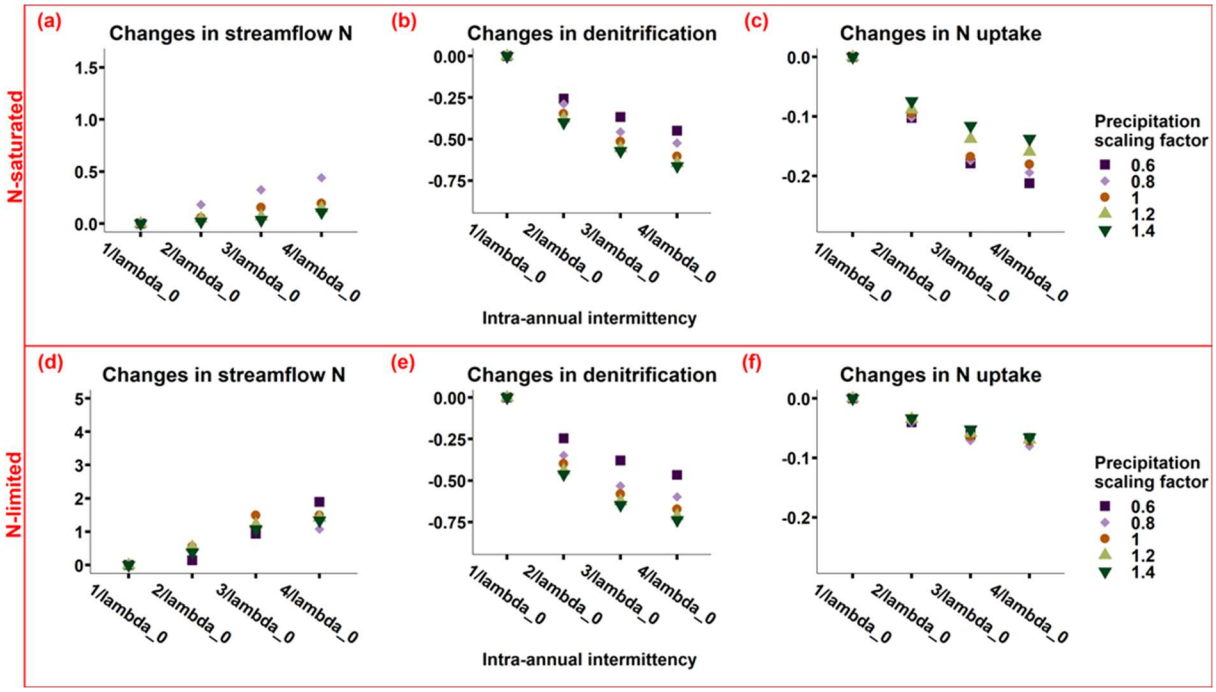

Figure 5. Sensitivity of cumulative N fluxes over 60 years to intra-annual precipitation intermittency for N-saturated and N-limited scenarios (normalized differences relative to baseline (1/λ_0). The x-axis is intermittency, the y-axis is normalized change of other intermittencies relative to their baseline intermittency scenarios (1/λ_0) for every precipitation scaling factor (different precipitation scaling factor scenarios have different baseline intermittency scenarios). The top panels are N-saturated and bottom panels are N-limited scenarios.

3.2.2 The effects of interannual precipitation intermittency on N export.

Greater interannual intermittency and higher levels of precipitation increased streamflow N export and this effect was consistent across both N-limited and N-saturated scenarios (Figure 6). Denitrification exhibited two distinct responses to interannual intermittency. First, when the intermittency exceeded 2/ λ_0, there was a significant increase in denitrification, which occurred because higher interannual intermittency corresponded with more precipitation per rainfall event, resulting in higher soil moisture levels across the landscape and triggering denitrification in non-hotspot patches (Figure 6b, e). However, denitrification started decreasing once interannual intermittency was larger than 3/ λ_0. At the highest interannual intermittency levels, increasing the duration of dry months decreased denitrification to a greater extent than larger storms

increased it. Plant uptake generally decreased with higher levels of interannual intermittency, which occurred because long-term drought slowed plant growth (Figure S4b). It is worth noting that the magnitude of streamflow N and denitrification in interannual intermittency scenarios is much larger than that of the scenarios for intra-annual intermittency (Figure 4 and Figure 6).

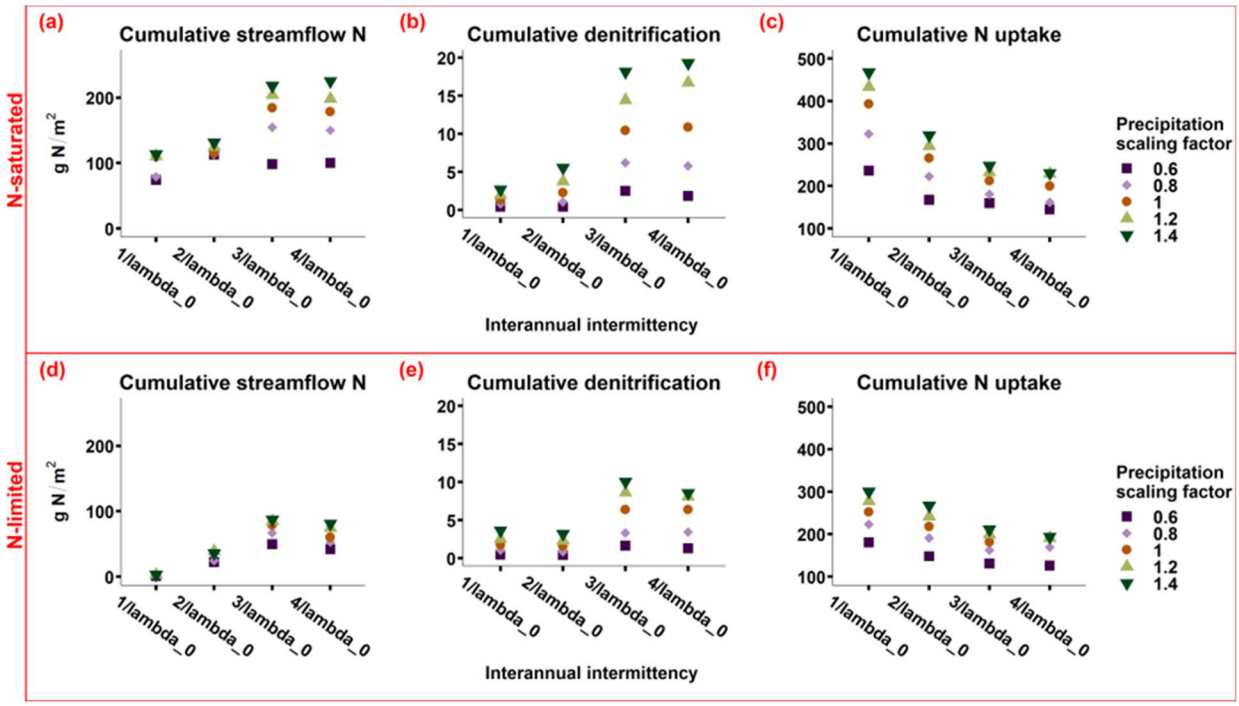

Figure 6. Sensitivity of cumulative N fluxes over 60 years (absolute value) to interannual precipitation intermittency for N-saturated and N-limited scenarios. The x-axis is the duration of dry days between rainfall events. Interannual intermittency increases from left to right.

Denitrification and plant N uptake were slightly more sensitive to interannual intermittency in N-saturated scenarios than in N-limited scenarios (Figure 7). This occurred because changes in denitrification and plant growth were constrained by N availability in N-limited scenarios and therefore less responsive to precipitation changes. Streamflow N export was more sensitive to interannual intermittency in N-limited scenarios compared to N-saturated scenarios (Figure 7a, d). In N-limited scenarios, drier scenarios showed greater changes to interannual intermittency than wetter scenarios, while in N-saturated scenarios wetter scenarios

showed greater changes. This occurred because in N-limited scenarios, drier scenarios had less denitrification and plant uptake, resulting in more N available to be flushed to the stream. It worth noting that in the N-limited scenario, interannual precipitation intermittency caused the largest changes in streamflow N export compared to intra-annual intermittency and interannual variability.

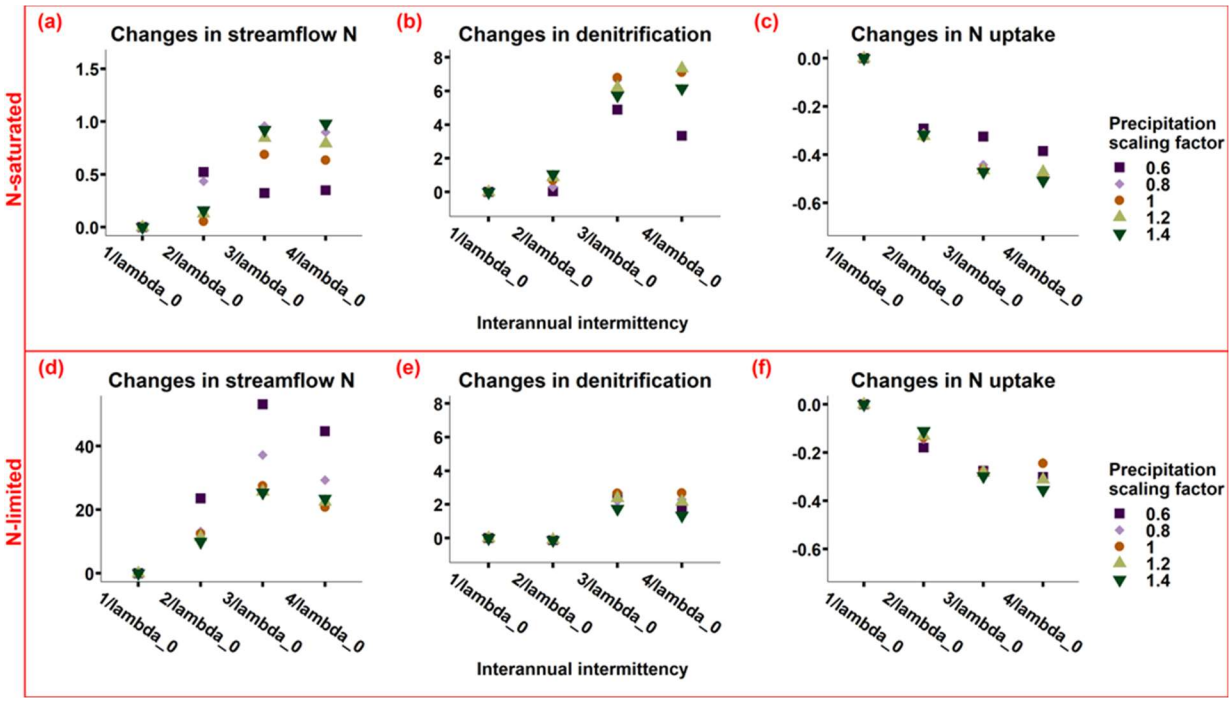

Figure 7. Sensitivity of cumulative N fluxes over 60 years to interannual precipitation intermittency for N-saturated and N-limited scenarios (differences are relative to baseline intermittency; 1/λ_0). The x-axis is intermittency, the y-axis is normalized change of other intermittencies relative to their baseline intermittency scenarios (1/λ_0) for every precipitation scaling factor. The top panels are N limited and the bottom panels are N saturated scenarios. Note that the scale of y-axis for changes in streamflow N is different for N-saturated and N-limited scenarios.

3.2.3 The effect of interannual precipitation variability on N export

In general, scenarios with higher precipitation variance and wetter scaling factors resulted in more streamflow N export (Figure 8). However, for wetter future scenarios, a precipitation scaling factor of 1.2 (rather than 1.4) resulted in the highest streamflow N export (Figure 8a, d).

This suggests there is a threshold of precipitation increase above which higher flushing capacity is compensated by less available N for flushing with higher denitrification and plant uptake. This can occur because more precipitation can cause higher denitrification and plant N uptake, which can reduce the amount of N available for flushing. Moreover, denitrification rates increased with higher precipitation variance and a higher precipitation scaling factor (Figure 8b, e). Notably, both streamflow N export and denitrification rates were higher in N-saturated compared to N-limited scenarios, due to greater nitrate inputs in N-saturated scenarios.

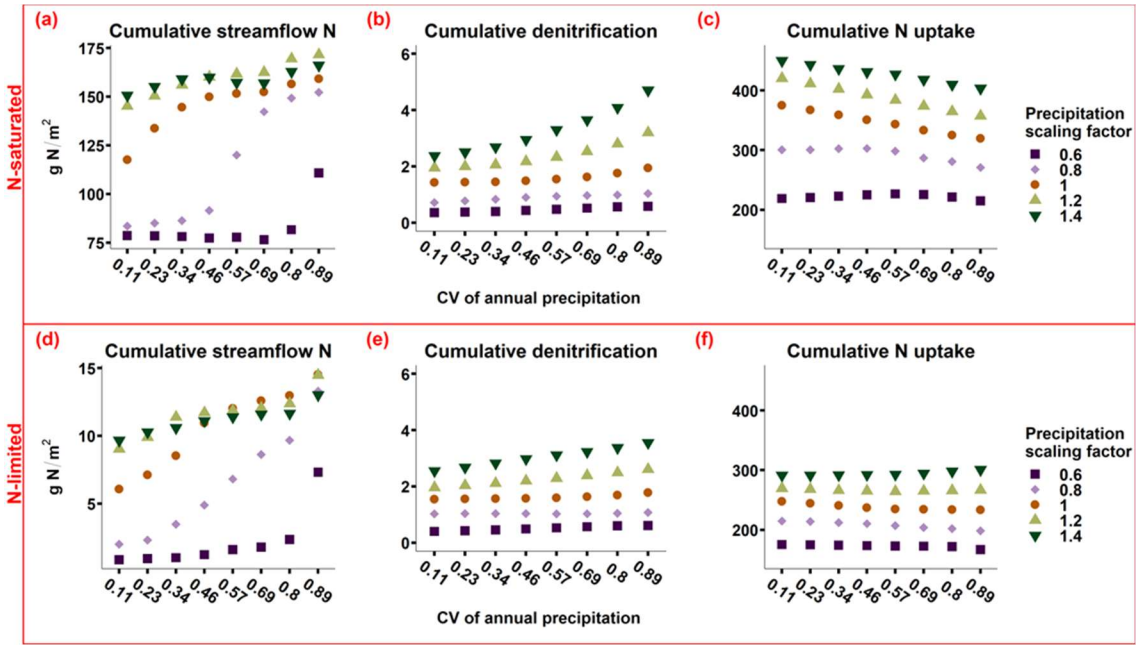

Figure 8. Cumulative N fluxes over 60 years (absolute value) relative to interannual precipitation variability and scaling factors for N-limited and N-saturated scenarios. The x axis is the coefficient of variation for annual precipitation, the y axis is the cumulative N fluxes over 60 years.

The sensitivity of N fluxes to precipitation variability differed between N-limited and N-saturated scenarios and was also affected by the precipitation scaling factors (i.e., drier vs. wetter futures; Figure 9). Streamflow N export was more sensitive to precipitation variability in N-limited than in N-saturated scenarios, particularly for the drier future scenarios (Figure 9a, d),

while denitrification showed the opposite trend (Figure 9b, e). The magnitude of sensitivity for plant N uptake was similar between N-limited and N-saturated scenarios, but the direction of effects (i.e., increases or decreases) differed and was affected by the precipitation scaling factor. In the N-limited scenarios, plant N uptake decreased with precipitation variability in drier future scenarios but increased in wetter future scenarios, suggesting that higher precipitation variability can increase plant growth when there is more water available, even if the watershed is N-limited. On the other hand, higher precipitation variability and water stress will suppress plant growth. In N-saturated scenarios, plant N uptake generally decreased with higher precipitation variability, except in some drier scenarios with smaller variability. This suggests that in N-saturated watersheds, less precipitation combined with moderately higher variability can promote plant growth to some extent.

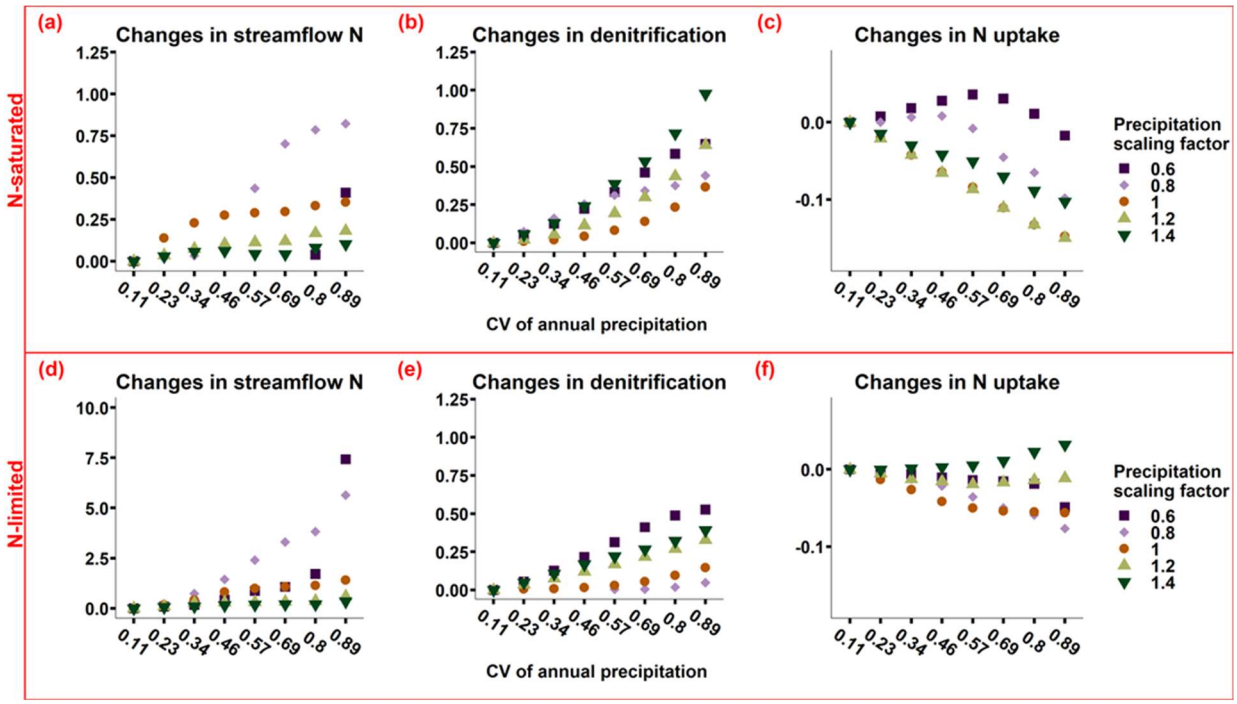

Figure 9. Sensitivity of cumulative N fluxes over 60 years to interannual precipitation variability for N-saturated and N-limited scenarios (differences are relative to the baseline variability scenario which is 0.11). The x axis is the coefficient of variation for annual precipitation. The y

axis is the normalized change in other variances relative to the baseline variability scenario (CV is 0.11) for every precipitation scaling factor (different precipitation scaling factor scenarios have different 0.1 variance baseline scenario). The top panels are N-saturated and the bottom panels are N-limited scenarios.

4 Discussion

Over the last century, atmospheric N deposition and climate change have increased both greenhouse gas emissions (e.g., NO and nitrous oxide; N_2O) and stream nitrate export from many dryland watersheds in western North America (Groffman, 2012; Homyak et al., 2016; Krichels et al., 2022). Because these gaseous and hydrologic N fluxes can exacerbate global climate change, decrease aquatic biodiversity, and harm human health (Galloway et al., 2003; Gustine et al., 2022; Meyer et al., 2022), it is important to be able to predict how they will change in the future. In drylands, N export is highly sensitive to both N deposition rates and precipitation variability (Welter et al., 2005; Ye & Grimm, 2013); interannual precipitation variability and intermittency are both projected to increase in drylands under future climate change (Pörtner et al., 2022). However, our ability to model and predict future N export remains limited, particularly in response to these interacting drivers.

Previous research has mainly focused on how the amount of precipitation in storm events can affect ecosystem function (e.g., Jarvis et al., 2007; Kennedy et al., 2021; Stephens et al., 2020; Ye & Grimm, 2013); fewer studies have also explored the cumulative effects of precipitation variability across multiple decades (D'Odorico et al., 2003; Gherardi & Sala, 2015; Jiang et al., 2019; Porporato et al., 2003). Further research is needed to examine how different types of precipitation intensification (e.g., increasing intermittency vs. variability) will influence biogeochemical cycling, and to investigate how these effects can differ between N-limited and N-saturated watersheds. In this study, we conducted a modeling analysis to understand how N saturation status, precipitation intermittency, variability, and the total amount of precipitation can

555 interact to influence N export in a dryland watershed in California. We found that streamflow N
556 was more sensitive to intensification of the precipitation regime in N-limited than N-limited
557 scenarios, whereas the opposite was true for denitrification. Furthermore, changes in interannual
558 precipitation intermittency had the largest effect on streamflow N and denitrification, suggesting
559 that N export may become an even greater threat to water quality when prolonged drought is
560 followed by more intense storm events.

561 **4.1 Identifying N deposition thresholds for capacity saturation**

562 To distinguish between kinetic (i.e., seasonal) and capacity (i.e., long-term) N saturation
563 (Lovett & Goodale 2011), we developed a simulation modeling approach that quantifies
564 watershed responses to N deposition under different rainfall seasonality regimes. By identifying
565 the amount of N deposition required for precipitation regimes to no longer modify N export, we
566 can approximate when N deposition has truly exceeded the capacity for plants and microbes to
567 take it up. This approach assumes that kinetic N saturation is more sensitive to precipitation
568 seasonality and timing, which affects plant and microbial N assimilation, while capacity N
569 saturation is less sensitive.

570 We found that the Bell 4 watershed can become capacity saturated when N deposition
571 reaches 2 g m^{-2} $year^{-1}$ over about 40 years (Figure 3). This suggests that the watershed—which
572 has a current mean N deposition rate greater than 2 g m^{-2} $year^{-1}$—has already approached
573 capacity saturation. It is important to note that the threshold we identified is location-specific and
574 is likely to vary with the size, vegetation cover, and climate of a given watershed (Dijkstra et al.,
575 2004; Yu et al., 2018). On average, N deposition is around 0.7 g m^{-2} $year^{-1}$ in dryland watersheds
576 globally and rates are expected to double by 2050 (Benish et al., 2022; Galloway et al., 2008;
577 Kanakidou et al., 2016). Given these increases, many other dryland watersheds could begin to

exceed the N deposition thresholds required to shift from a kinetic to capacity saturation in the coming decades. These shifts can pose a major threat to water quality, aquatic ecosystems, and human health. Our study provides a useful modeling approach that can be applied to other watersheds to determine N deposition thresholds for establishing capacity N saturation.

4.2 The role of N saturation status

Does an increase in N deposition lead to greater N export or N uptake? It is essential to distinguish between N-saturated and N-limited watersheds to unravel how changes in the total amount of precipitation and its intermittency or variability will influence watershed processes (Rudgers et al., 2023). In our model setup, N deposition was 100 times higher in N-saturated than in N-limited scenarios. However, the N-saturated/N-limited ratios for various N fluxes (i.e., streamflow N, denitrification, N uptake) were all smaller than 100 and varied among scenarios (Figure S5). This suggests that N partitioning and soil N storage also changed in response to N-deposition. Not surprisingly, streamflow N had the highest N-saturated/N-limited ratios, ranging from 15 to 80. Denitrification and N uptake, on the other hand, only experienced modest 1-2-fold increases in response to N saturation (Figure S5). Because most atmospherically deposited N is exported to streams, projected decreases in streamflow (Ficklin et al., 2022; Stephens et al., 2020) could lead to even higher streamflow nitrate concentrations, particularly under increased interannual precipitation variability (Gallo et al., 2015; Ye & Grimm, 2013).

As precipitation regimes become more intermittent and/or variable, N-limited watersheds can retain less N in soil (Winter et al., 2023) and N saturated watershed can become more saturated or retain more N in soil . In N-limited scenarios, total N export was 25 times higher than the rate of atmospheric N deposition over the 60-year simulation period. This occurred in large part due to declines in plant productivity and N uptake. In N-saturated scenarios, on the

other hand, the ratio between N inputs and outputs was consistently less than one, with approximately 20% to 60% of the atmospheric N deposition being exported over the 60-year simulation period (Figure 10). The highest N export transfer efficiencies (calculated as the ratio between total N export and N deposition) occurred with high interannual intermittency, while high intra-annual intermittency produced the lowest. Additionally, transfer efficiency can become even higher in a wetter future due to increases in streamflow. Thus, in N-limited scenarios (particularly in a wetter future), increases in precipitation interannual intermittency can increase N export efficiency, thereby reducing N retention capacity in soil. However, our result should be interpreted with care since 25 times higher N transfer efficiency will eventually deplete the N in soil. Conversely, in N-saturated scenarios, a drier future will have lower transfer efficiencies, which can intensify N saturation. This is corroborated by a recent meta-analysis globally, which found that reduced precipitation can increase soil N storage over long-term studies, particularly precipitation decreases by more than 25% (Wu et al., 2022).

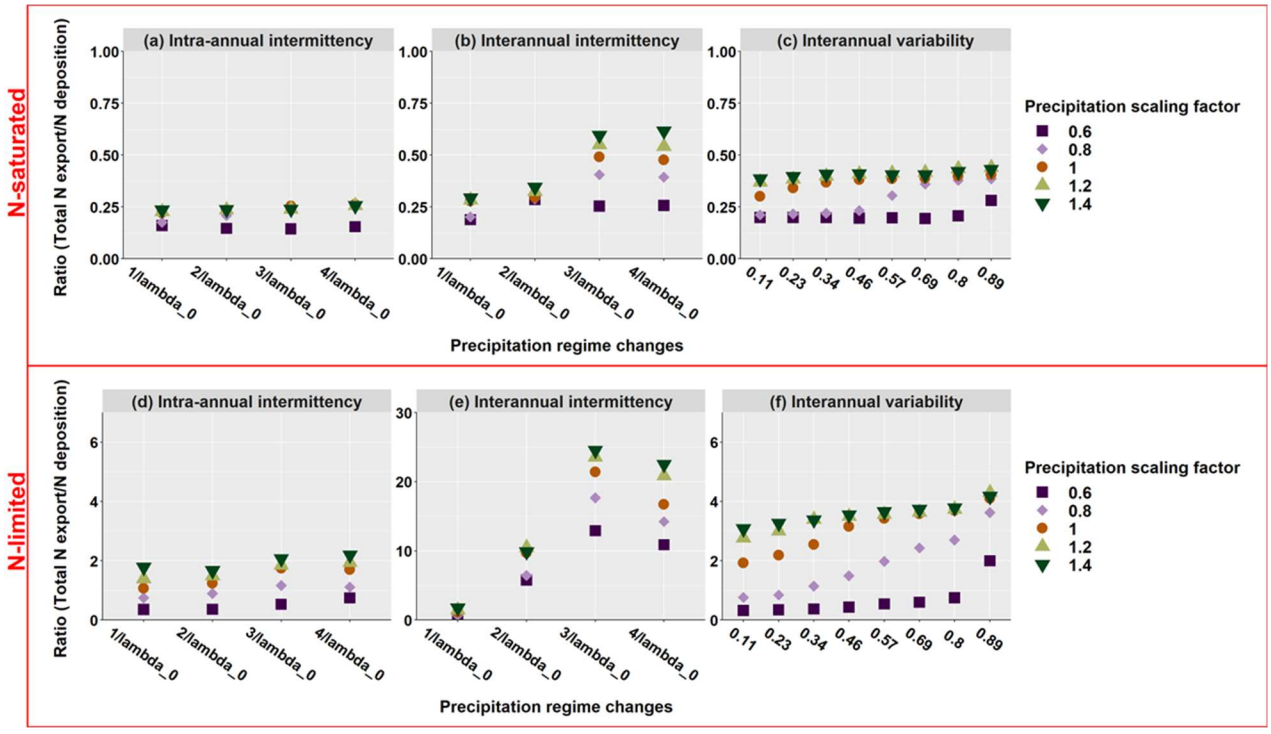

Figure 10. The ratio of total N export (streamflow N and denitrification) to N deposition and its response to precipitation regime changes. For N-saturated scenarios, the N deposition rate was 5 g m^{-2} $year^{-1}$, for N-limited scenarios, it was 0.05 g m^{-2} $year^{-1}$. Ratios larger than 1 indicates N outputs are larger than N inputs and vice versa.

4.3 The role of changing precipitation regimes

Recent studies have found that precipitation amount and variability both play an important role in driving ecosystem responses to climate change (Gherardi & Sala, 2015, 2019; Jiang et al., 2019; Rudgers et al., 2023). Here we extend those studies to also examine the role of precipitation intermittency and focus on how it affects streamflow N export. In our experimental setup, we ensured water balance among all scenarios (e.g., scenarios with high vs. low interannual intermittency at a given amount of total precipitation had the same total rainfall over the 60-year simulation period). Thus, longer droughts were followed by more precipitation after drought. Thus interannual intermittency scenarios varied both the timing of storms and their magnitude, whereas interannual precipitation variability scenarios only varied the relative magnitude of storms (e.g., some become larger and some become smaller with increasing variability; Figure 1c). We found that increases in interannual intermittency produced the largest increases (with the greatest variance) in streamflow N among precipitation regime scenarios (Figure 11a). Conversely, interannual variability had the smallest effect on streamflow N. These findings suggest that prolonged drought followed by larger, more intense storms can have the strongest effect on streamflow N. This occurs because multi-year droughts that occur with greater intermittency can reduce N uptake by plants and enable N to accumulate in soils (Krichels et al., 2022; Winter et al., 2023). Subsequent storms then flush accumulated N to streams before plants can take it up.

Denitrification exhibited the most substantial increases with increasing interannual intermittency, whereas it slightly decreased with increasing intra-annual intermittency (Figure

11b). This pattern arose because denitrification is strongly influenced by soil moisture and therefore the amount of precipitation in storm events (Homyak et al., 2016). Increases in both interannual intermittency and variability had large effects on the size of individual storms, while increases in intra-annual intermittency had relatively smaller effects.

Higher precipitation intra-annual and interannual intermittency and variability can both reduce plant growth and corresponding N uptake, but increases in interannual intermittency, which lead to fewer, more intense storms, exert a stronger influence than changes in variability alone (which only affects the relative size of storms without changing their timing). These findings have important implications for designing field and laboratory experiments aimed at understanding plant responses to changing precipitation regimes. Such experiments should not only consider the important roles of storm size and variance (as identified by Gherardi & Sala (2015) and Rudgers et al. (2023)), but should also incorporate intermittency as a key driver.

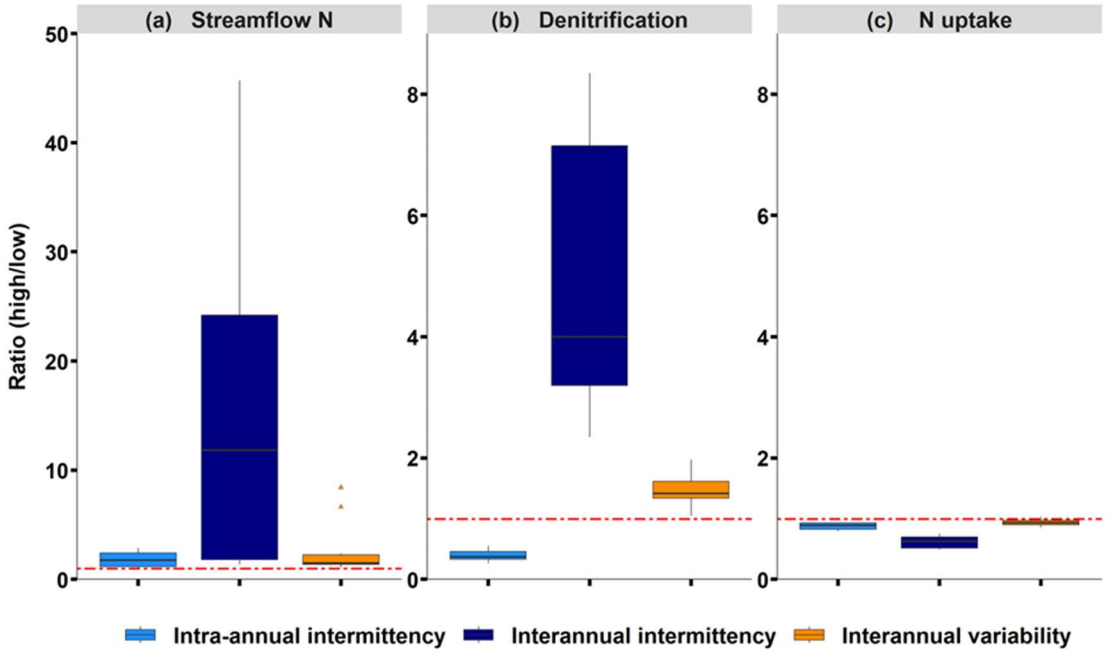

Figure 11. The distribution of ratios of highest intermittency/variability to lowest for different N fluxes. For intermittency this is the ratio between 4/lambda_0 and 1/lambda_0, for variability this is the ratio between 0.89 CV and 0.11 CV. The distribution consists of outputs from all N saturation and precipitation scaling factor scenarios and the variance of distribution indicates how sensitive these N fluxes were to intra-annual intermittency, interannual intermittency, and interannual variability. Note that the y-axis for panel a is on a different scale than for panels b and c. The red dashed line represents a ratio of 1, above which N fluxes increases with intensified precipitation regime and below 1 indicates a decrease.

4.4 The role of total precipitation amount in N-limited systems

Does more total precipitation result in higher N export? When transitioning from drier to wetter future scenarios, denitrification was the most affected, followed by streamflow N, while plant N uptake was least affected (Figure 12 d, e, and f). With a 2.3 fold increase of precipitation (from a 0.6 to a 1.4 scaling factor), median denitrification increased approximately 5 to 7 fold, and this response was slightly greater in N saturated scenarios compared to N-limited scenarios (Figure 12e). This finding aligns with the fact that denitrification is strongly influenced by soil moisture and available nitrate (Poblador et al., 2017). Denitrification is also strongly influenced by soil C (represented as a function of soil respiration in RHESSys), which was higher in wetter

future and N-saturated scenarios. Conversely, streamflow N in N-limited scenarios was more responsive to changes in the precipitation scaling factor than in N-saturated scenarios (Figure 12d). In N-limited scenarios, streamflow N increased the precipitation scaling factor, reaching approximately 3.5 times higher than baseline in scenarios with a scaling factor of 1.2. However, it reached an asymptote once the scaling factor exceeded 1.2. This suggests that, for N-limited scenarios, increases in total precipitation do not necessarily translate into higher streamflow N because additional water can enhance denitrification, plant N uptake, and reduce nitrification. Because the effects of total precipitation on streamflow N export are non-linear, it can be challenging to predict N export as precipitation regimes continue to change, particularly in N-limited watersheds (Harms & Grimm, 2008; Homyak et al., 2016).

Changes in the amount of precipitation can also interact with N saturation status to modify various N fluxes. For example, a higher precipitation scaling factor enhanced the N saturation effect on denitrification and its variability (Figure 12h). Alternatively, in drier future scenarios the ratio between N-saturated to N-limited denitrification was smaller than 1 (Figure 12h), suggesting that a drier future can largely inhibit (or even reverse) the N saturation effect, even with 100 times higher N deposition (Wu et al., 2022). With respect to streamflow N, a higher precipitation scaling factor reduced the effects of N saturation and its variability (Figure 12g). This aligns with predictions that a drier future would lead to greater N export to streams and a lower flux to the atmosphere through denitrification (Cregger et al., 2014). Our findings also corroborate recent studies showing that interactions between N deposition and the total amount of precipitation drive N export in drylands (Li et al., 2022).

Although increases or decreases in the total amount of precipitation had smaller effects on N fluxes than increases in intermittency and/or variability, they interacted with precipitation

timing to amplify or attenuate their effects. In N-limited scenarios, streamflow N export increased with higher intermittency and variability, but a drier future exaggerated this response whereas a wetter future dampened it (e.g., Figure 5d, Figure 7d, and Figure 9d). Although a wetter future may lead to greater overall streamflow N export (e.g., Figure 8d), a drier future can result in more substantial increases in streamflow N export (Figure 9d). Furthermore, even minor decreases in the precipitation scaling factor could substantially increase streamflow N (e.g., Figure 9d and Figure 12g; 0.8 and 0.6 precipitation scaling factors). Thus, the total amount of precipitation can play a critical threshold role in driving how N fluxes respond to increases in precipitation variability and timing (Ficklin et al., 2022).

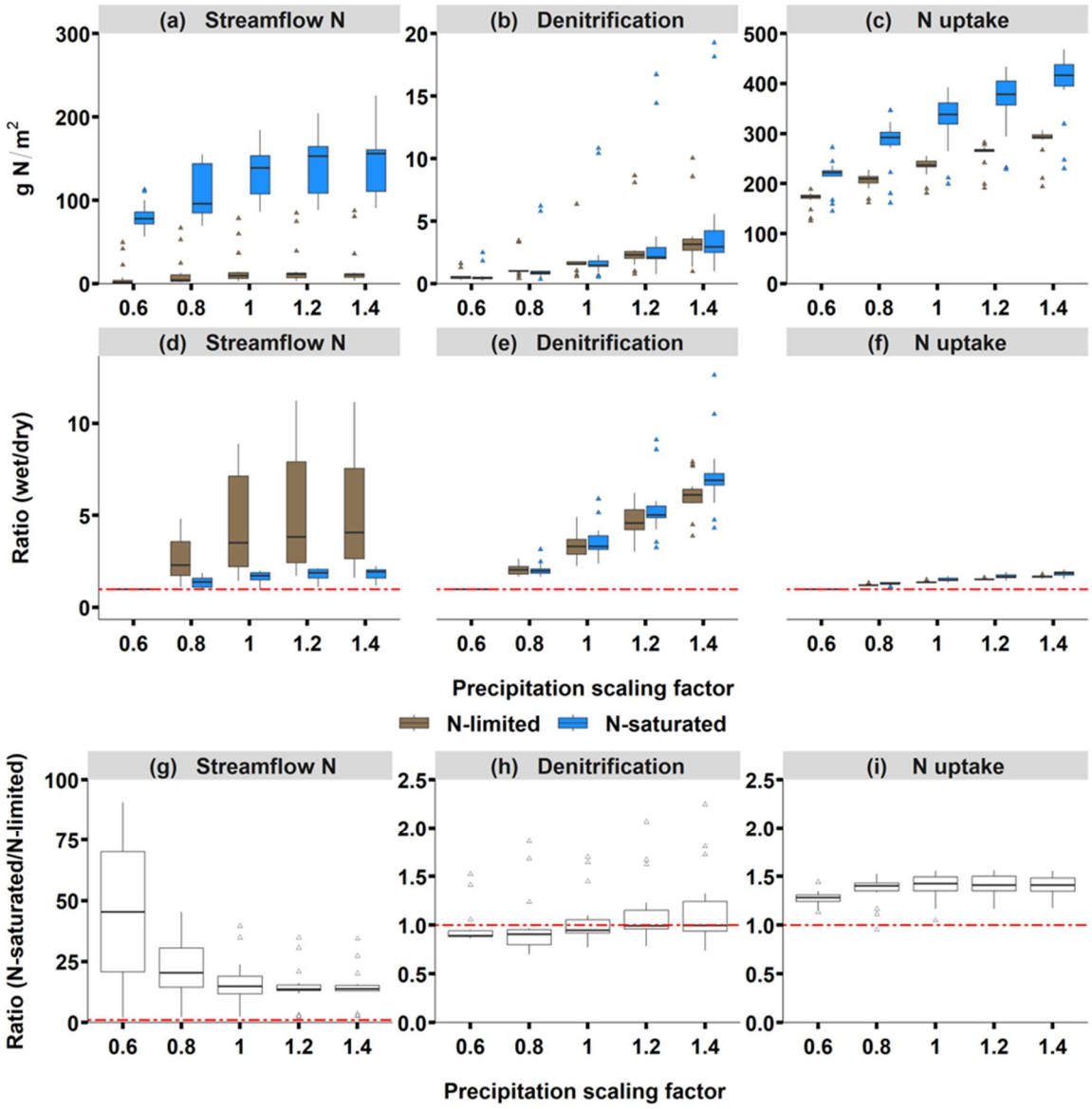

Figure 12. The effect of drier or wetter conditions on N fluxes. The top panels a, b, and c represent how cumulative N fluxes over 60 years change with precipitation scaling factor. Each distribution contains both N saturation statuses and all precipitation regime changes. The middle panels of d, e, and f represent the ratio of fluxes between precipitation scaling factors larger than 0.6 and the driest scaling factor (i.e., 0.6). The bottom panels g, h and i represent the ratio of fluxes in N-saturated and N-limited conditions and how they vary with the precipitation scaling factor. The dashed blue line denotes a ratio equal to 1.

4.5 Study implications

Predicting future N export in drylands requires considering interaction between hotspots (defined as wetter microsites in the soil that have disproportionately high rates of

713 biogeochemical cycling) and hot moments (defined as wet periods after a prolonged dry spell)
714 rather than treating them as separate entities (Groffman et al., 2009; Kuzyakov & Blagodatskaya,
715 2015; Pinay et al., 2015). Our study revealed that the interannual intermittency exhibited the
716 largest influence on streamflow N and denitrification. Interannual intermittency scenarios
717 incorporated increases in both the timing and magnitude of storms (with the same total
718 precipitation over the simulation period for a given precipitation multiplier). Following
719 prolonged drought, large storms can be viewed as hot moments. Once the amount of
720 precipitation during these hot moments surpassed a certain threshold (e.g., $2/\lambda$ in Figure 7e),
721 denitrification was activated in patches across the basin that were not designated as microscale
722 hotspots. This generated a more dynamic distribution of "hotspots" due to the timing of hot
723 moments. To better account for the interdependence between hotspots and hot moments,
724 Bernhardt et al. (2017) proposed a new term more comprehensive term: "ecosystem control
725 points." This new term incorporates both spatial and temporal dynamics instead of addressing
726 them independently (Bernhardt et al., 2017). Our research in a dryland chaparral watershed
727 illustrates how ecosystem control points drive N export under a range of future scenarios.

728 Our modeling framework considered interactions between N saturation status and several
729 ways that precipitation regimes can change. This framework can serve as a tool for
730 understanding the specific mechanisms driving future N export under climate change. For
731 example, our model framework highlights the importance of considering the role of interannual
732 intermittency (not just variability) when examining how future precipitation will influence N
733 fluxes. This approach can help researcher determine the interannual intermittency thresholds that
734 trigger substantial increases in denitrification, which can in turn help them design precipitation
735 manipulation experiments with appropriate intermittency levels.

5 Conclusion

We developed a comprehensive modeling framework that incorporates the role of both N deposition and intensification of the precipitation regime (i.e., the total amount, intermittency, and variability) in driving N export in dryland ecosystems. We identified a critical N deposition threshold of around 2 g m^{-2} $year^{-1}$ beyond which the watershed shifts from N-limited to N-saturated. Our findings reveal that streamflow N export in N-limited watersheds is more sensitive to changes in the timing of precipitation compared to N-saturated watersheds, whereas denitrification in N-saturated watersheds was more responsive to changes in precipitation timing in N-saturated watersheds. Additionally, we found that a drier future exaggerated the effects of precipitation timing on N export, while there was no uniform response under a wetter future. Notably, among the various precipitation regime changes, interannual intermittency caused the largest changes in N export compared to other characteristics of the precipitation regime. Our modeling framework helps disentangle the key drivers of N fluxes amid complex interactions between N saturation and precipitation in dryland watersheds. We found that interannual rainfall intermittency enables solutes like nitrate to build up in hotspots and then be flushed to streams with subsequent intense storms—thus as rainfall intermittency and associated droughts continue to increase, N export will become an even greater threat to water security.

6 Acknowledgments

This project was supported by National Science Foundation of the United States under award number DEB-1916658. We thank Tom Dilts for helping with preparing input maps and data of RHESSys. We thank Pete Wohlgemuth for helping with streamflow data processing and model calibration.

Data Availability Statement

The data sets used to run simulations for this study can be found in the Open Science Forum: https://doi.org/10.17605/OSF.IO/7QTXV, and the model code can be found on GitHub: https://doi.org/10.5281/zenodo.7754375.

References

Abatzoglou, J. T. (2013). Development of gridded surface meteorological data for ecological applications and modelling. *International Journal of Climatology*, *33*(1), 121–131. https://doi.org/10.1002/joc.3413

Aber, J. D., Nadelhoffer, K. J., Steudler, P., & Melillo, J. M. (1989). Nitrogen Saturation in Northern Forest Ecosystems: Excess nitrogen from fossil fuel combustion may stress the biosphere. *BioScience*, *39*(6), 378–386. https://doi.org/10.2307/1311067

Allen, M. R., & Ingram, W. J. (2002). Constraints on future changes in climate and the hydrologic cycle. *Nature*, *419*(6903), 224–232. https://doi.org/10.1038/nature01092

Benish, S. E., Bash, J. O., Foley, K. M., Appel, K. W., Hogrefe, C., Gilliam, R., & Pouliot, G. (2022). Long-term regional trends of nitrogen and sulfur deposition in the United States from 2002 to 2017. *Atmospheric Chemistry and Physics*, *22*(19), 12749–12767. https://doi.org/10.5194/acp-22-12749-2022

Bernhardt, E. S., Blaszczak, J. R., Ficken, C. D., Fork, M. L., Kaiser, K. E., & Seybold, E. C. (2017). Control Points in Ecosystems: Moving Beyond the Hot Spot Hot Moment Concept. *Ecosystems*, *20*(4), 665–682. https://doi.org/10.1007/s10021-016-0103-y

Burke, W. D., Tague, C., Kennedy, M. C., & Moritz, M. A. (2021). Understanding How Fuel Treatments Interact With Climate and Biophysical Setting to Affect Fire, Water, and

Forest Health: A Process-Based Modeling Approach. *Frontiers in Forests and Global Change*, *3*. https://doi.org/10.3389/ffgc.2020.591162

Bytnerowicz, A., & Fenn, M. E. (1996). Nitrogen deposition in California forests: a review. *Environmental Pollution, Vol. 92(2): 127-146*. Retrieved from https://www.fs.usda.gov/research/treesearch/24944

Chaney, N. W., Wood, E. F., McBratney, A. B., Hempel, J. W., Nauman, T. W., Brungard, C. W., & Odgers, N. P. (2016). POLARIS: A 30-meter probabilistic soil series map of the contiguous United States. *Geoderma*, *274*, 54–67. https://doi.org/10.1016/j.geoderma.2016.03.025

Chen, X., Tague, C. L., Melack, J. M., & Keller, A. A. (2020). Sensitivity of nitrate concentration-discharge patterns to soil nitrate distribution and drainage properties in the vertical dimension. *Hydrological Processes*, *34*(11), 2477–2493. https://doi.org/10.1002/hyp.13742

Cregger, M. A., McDowell, N. G., Pangle, R. E., Pockman, W. T., & Classen, A. T. (2014). The impact of precipitation change on nitrogen cycling in a semi-arid ecosystem. *Functional Ecology*, *28*(6), 1534–1544. https://doi.org/10.1111/1365-2435.12282

Dentener, F., Drevet, J., Lamarque, J. F., Bey, I., Eickhout, B., Fiore, A. M., et al. (2006). Nitrogen and sulfur deposition on regional and global scales: A multimodel evaluation. *Global Biogeochemical Cycles*, *20*(4). https://doi.org/10.1029/2005GB002672

Dickinson, R. E., Shaikh, M., Bryant, R., & Graumlich, L. (1998). Interactive Canopies for a Climate Model. *Journal of Climate*, *11*(11), 2823–2836. https://doi.org/10.1175/1520-0442(1998)011<2823:ICFACM>2.0.CO;2

802 Dijkstra, F. A., Hobbie, S. E., Knops, J. M. H., & Reich, P. B. (2004). Nitrogen deposition and
803 plant species interact to influence soil carbon stabilization. *Ecology Letters*, *7*(12), 1192–
804 1198. https://doi.org/10.1111/j.1461-0248.2004.00679.x
805 D'Odorico, P., Laio, F., Porporato, A., & Rodriguez-Iturbe, I. (2003). Hydrologic controls on
806 soil carbon and nitrogen cycles. II. A case study. *Advances in Water Resources*, *26*(1),
807 59–70. https://doi.org/10.1016/S0309-1708(02)00095-7
808 Dunn, P. H., Barro, S. C., Wells, W. G., Poth, M. A., Wohlgemuth, P. M., & Colver, C. G.
809 (1988). *The San Dimas experimental forest: 50 years of research* (No. PSW-GTR-104)
810 (p. PSW-GTR-104). Berkeley, CA: U.S. Department of Agriculture, Forest Service,
811 Pacific Southwest Forest and Range Experiment Station. https://doi.org/10.2737/PSW-
812 GTR-104
813 Eagleson, P. S. (1978). Climate, soil, and vegetation: 3. A simplified model of soil moisture
814 movement in the liquid phase. *Water Resources Research*, *14*(5), 722–730.
815 https://doi.org/10.1029/WR014i005p00722
816 Farquhar, G. D., & von Caemmerer, S. (1982). Modelling of Photosynthetic Response to
817 Environmental Conditions. In O. L. Lange, P. S. Nobel, C. B. Osmond, & H. Ziegler
818 (Eds.), *Physiological Plant Ecology II: Water Relations and Carbon Assimilation* (pp.
819 549–587). Berlin, Heidelberg: Springer. https://doi.org/10.1007/978-3-642-68150-9_17
820 Ficklin, D. L., Null, S. E., Abatzoglou, J. T., Novick, K. A., & Myers, D. T. (2022).
821 Hydrological Intensification Will Increase the Complexity of Water Resource
822 Management. *Earth's Future*, *10*(3), e2021EF002487.
823 https://doi.org/10.1029/2021EF002487

824 Fischer, E. M., Beyerle, U., & Knutti, R. (2013). Robust spatially aggregated projections of
825 climate extremes. *Nature Climate Change*, *3*(12), 1033–1038.
826 https://doi.org/10.1038/nclimate2051
827 Gallo, E. L., Meixner, T., Aoubid, H., Lohse, K. A., & Brooks, P. D. (2015). Combined impact
828 of catchment size, land cover, and precipitation on streamflow and total dissolved
829 nitrogen: A global comparative analysis. *Global Biogeochemical Cycles*, *29*(7), 1109–
830 1121. https://doi.org/10.1002/2015GB005154
831 Galloway, J. N., Aber, J. D., Erisman, J. W., Seitzinger, S. P., Howarth, R. W., Cowling, E. B.,
832 & Cosby, B. J. (2003). The Nitrogen Cascade. *BioScience*, *53*(4), 341–356.
833 https://doi.org/10.1641/0006-3568(2003)053[0341:TNC]2.0.CO;2
834 Galloway, J. N., Townsend, A. R., Erisman, J. W., Bekunda, M., Cai, Z., Freney, J. R., et al.
835 (2008). Transformation of the Nitrogen Cycle: Recent Trends, Questions, and Potential
836 Solutions. *Science*, *320*(5878), 889–892. https://doi.org/10.1126/science.1136674
837 Garcia, E. S., & Tague, C. L. (2015). Subsurface storage capacity influences climate–
838 evapotranspiration interactions in three western United States catchments. *Hydrology and*
839 *Earth System Sciences*, *19*(12), 4845–4858. https://doi.org/10.5194/hess-19-4845-2015
840 Garcia, Elizabeth S., Tague, C. L., & Choate, J. S. (2016). Uncertainty in carbon allocation
841 strategy and ecophysiological parameterization influences on carbon and streamflow
842 estimates for two western US forested watersheds. *Ecological Modelling*, *342*, 19–33.
843 https://doi.org/10.1016/j.ecolmodel.2016.09.021
844 Gherardi, L. A., & Sala, O. E. (2015). Enhanced precipitation variability decreases grass- and
845 increases shrub-productivity. *Proceedings of the National Academy of Sciences*, *112*(41),
846 12735–12740. https://doi.org/10.1073/pnas.1506433112

847 Gherardi, L. A., & Sala, O. E. (2019). Effect of interannual precipitation variability on dryland
848 productivity: A global synthesis. *Global Change Biology*, *25*(1), 269–276.
849 https://doi.org/10.1111/gcb.14480
850 Groffman, P. M. (2012). Terrestrial denitrification: challenges and opportunities. *Ecological*
851 *Processes*, *1*(1), 1–11. https://doi.org/10.1186/2192-1709-1-11
852 Groffman, P. M., Butterbach-bahl, K., Fulweiler, R. W., Gold, A. J., Morse, J. L., Stander, E. K.,
853 et al. (2009). Challenges to incorporating spatially and temporally explicit phenomena
854 (hotspots and hot moments) in denitrification models. *Biogeochemistry*, *93*(1–2), 49–77.
855 https://doi.org/10.1007/s10533-008-9277-5
856 Gustine, R. N., Hanan, E. J., Robichaud, P. R., & Elliot, W. J. (2022). From burned slopes to
857 streams: how wildfire affects nitrogen cycling and retention in forests and fire-prone
858 watersheds. *Biogeochemistry*, *157*(1), 51–68. https://doi.org/10.1007/s10533-021-00861-
859 0
860 Hanan, E. J., Tague, C. (Naomi), & Schimel, J. P. (2017). Nitrogen cycling and export in
861 California chaparral: the role of climate in shaping ecosystem responses to fire.
862 *Ecological Monographs*, *87*(1), 76–90. https://doi.org/10.1002/ecm.1234
863 Hanan, E. J., Tague, C., Choate, J., Liu, M., Kolden, C., & Adam, J. (2018). Accounting for
864 disturbance history in models: using remote sensing to constrain carbon and nitrogen pool
865 spin-up. *Ecological Applications: A Publication of the Ecological Society of America*,
866 *28*(5), 1197–1214. https://doi.org/10.1002/eap.1718
867 Hanan, E. J., Ren, J., Tague, C. L., Kolden, C. A., Abatzoglou, J. T., Bart, R. R., et al. (2021).
868 How climate change and fire exclusion drive wildfire regimes at actionable scales.

Environmental Research Letters, *16*(2), 024051. https://doi.org/10.1088/1748-9326/abd78e

Harms, T. K., & Grimm, N. B. (2008). Hot spots and hot moments of carbon and nitrogen dynamics in a semiarid riparian zone. *Journal of Geophysical Research: Biogeosciences*, *113*(G1). https://doi.org/10.1029/2007JG000588

Homyak, P. M., Sickman, J. O., Miller, A. E., Melack, J. M., Meixner, T., & Schimel, J. P. (2014). Assessing Nitrogen-Saturation in a Seasonally Dry Chaparral Watershed: Limitations of Traditional Indicators of N-Saturation. *Ecosystems*, *17*(7), 1286–1305. https://doi.org/10.1007/s10021-014-9792-2

Homyak, P. M., Blankinship, J. C., Marchus, K., Lucero, D. M., Sickman, J. O., & Schimel, J. P. (2016). Aridity and plant uptake interact to make dryland soils hotspots for nitric oxide (NO) emissions. *Proceedings of the National Academy of Sciences*, *113*(19), E2608–E2616. https://doi.org/10.1073/pnas.1520496113

Homyak, P. M., Allison, S. D., Huxman, T. E., Goulden, M. L., & Treseder, K. K. (2017). Effects of Drought Manipulation on Soil Nitrogen Cycling: A Meta-Analysis. *Journal of Geophysical Research: Biogeosciences*, *122*(12), 3260–3272. https://doi.org/10.1002/2017JG004146

Howarth, R. W., Swaney, D. P., Boyer, E. W., Marino, R., Jaworski, N., & Goodale, C. (2006). The influence of climate on average nitrogen export from large watersheds in the Northeastern United States. *Biogeochemistry*, *79*(1), 163–186. https://doi.org/10.1007/s10533-006-9010-1

Hubbert, K. R., Preisler, H. K., Wohlgemuth, P. M., Graham, R. C., & Narog, M. G. (2006). Prescribed burning effects on soil physical properties and soil water repellency in a steep

chaparral watershed, southern California, USA. *Geoderma*, *130*(3), 284–298. https://doi.org/10.1016/j.geoderma.2005.02.001

Jarvis, P., Rey, A., Petsikos, C., Wingate, L., Rayment, M., Pereira, J., et al. (2007). Drying and wetting of Mediterranean soils stimulates decomposition and carbon dioxide emission: the "Birch effect." *Tree Physiology*, *27*(7), 929–940. https://doi.org/10.1093/treephys/27.7.929

Jiang, P., Liu, H., Piao, S., Ciais, P., Wu, X., Yin, Y., & Wang, H. (2019). Enhanced growth after extreme wetness compensates for post-drought carbon loss in dry forests. *Nature Communications*, *10*(1), 195. https://doi.org/10.1038/s41467-018-08229-z

Kanakidou, M., Myriokefalitakis, S., Daskalakis, N., Fanourgakis, G., Nenes, A., Baker, A. R., et al. (2016). Past, Present and Future Atmospheric Nitrogen Deposition. *Journal of the Atmospheric Sciences*, *73*(5), 2039–2047. https://doi.org/10.1175/JAS-D-15-0278.1

Kennedy, M. C., Bart, R. R., Tague, C. L., & Choate, J. S. (2021). Does hot and dry equal more wildfire? Contrasting short- and long-term climate effects on fire in the Sierra Nevada, CA. *Ecosphere*, *12*(7), e03657. https://doi.org/10.1002/ecs2.3657

Knapp, A. K., Fay, P. A., Blair, J. M., Collins, S. L., Smith, M. D., Carlisle, J. D., et al. (2002). Rainfall Variability, Carbon Cycling, and Plant Species Diversity in a Mesic Grassland. *Science*, *298*(5601), 2202–2205.

Knapp, A. K., Hoover, D. L., Wilcox, K. R., Avolio, M. L., Koerner, S. E., La Pierre, K. J., et al. (2015). Characterizing differences in precipitation regimes of extreme wet and dry years: implications for climate change experiments. *Global Change Biology*, *21*(7), 2624–2633. https://doi.org/10.1111/gcb.12888

914 Krichels, A. H., Greene, A. C., Jenerette, G. D., Spasojevic, M. J., Glassman, S. I., & Homyak,
915 P. M. (2022). Precipitation legacies amplify ecosystem nitrogen losses from nitric oxide
916 emissions in a Pinyon–Juniper dryland. *Ecology*, *104*(2), e3930.
917 https://doi.org/10.1002/ecy.3930
918 Kuzyakov, Y., & Blagodatskaya, E. (2015). Microbial hotspots and hot moments in soil:
919 Concept & review. *Soil Biology and Biochemistry*, *83*, 184–199.
920 https://doi.org/10.1016/j.soilbio.2015.01.025
921 Li, Z., Tang, Z., Song, Z., Chen, W., Tian, D., Tang, S., et al. (2022). Variations and controlling
922 factors of soil denitrification rate. *Global Change Biology*, *28*(6), 2133–2145.
923 https://doi.org/10.1111/gcb.16066
924 Lin, L., Webster, J. R., Hwang, T., & Band, L. E. (2015). Effects of lateral nitrate flux and
925 instream processes on dissolved inorganic nitrogen export in a forested catchment: A
926 model sensitivity analysis. *Water Resources Research*, *51*(4), 2680–2695.
927 https://doi.org/10.1002/2014WR015962
928 Lovett, G. M., & Goodale, C. L. (2011). A New Conceptual Model of Nitrogen Saturation Based
929 on Experimental Nitrogen Addition to an Oak Forest. *Ecosystems*, *14*(4), 615–631.
930 https://doi.org/10.1007/s10021-011-9432-z
931 Maxwell, A. E., Warner, T. A., Vanderbilt, B. C., & Ramezan, C. A. (2017). Land Cover
932 Classification and Feature Extraction from National Agriculture Imagery Program
933 (NAIP) Orthoimagery: A Review. *Photogrammetric Engineering & Remote Sensing*,
934 *83*(11), 737–747. https://doi.org/10.14358/PERS.83.10.737
935 Meyer, M. F., Ozersky, T., Woo, K. H., Shchapov, K., Galloway, A. W. E., Schram, J. B., et al.
936 (2022). Effects of spatially heterogeneous lakeside development on nearshore biotic

communities in a large, deep, oligotrophic lake. *Limnology and Oceanography*, *67*(12), 2649–2664. https://doi.org/10.1002/lno.12228

Nash, J. E., & Sutcliffe, J. V. (1970). River flow forecasting through conceptual models part I — A discussion of principles. *Journal of Hydrology*, *10*(3), 282–290. https://doi.org/10.1016/0022-1694(70)90255-6

Parker, S. S., & Schimel, J. P. (2011). Soil nitrogen availability and transformations differ between the summer and the growing season in a California grassland. *Applied Soil Ecology*, *48*(2), 185–192. https://doi.org/10.1016/j.apsoil.2011.03.007

Parton, W. J. (1996). The CENTURY model. In D. S. Powlson, P. Smith, & J. U. Smith (Eds.), *Evaluation of Soil Organic Matter Models* (Vol. 38, pp. 283–291). Springer, Berlin, Heidelberg: Evaluation of Soil Organic Matter Models.

Pinay, G., Peiffer, S., De Dreuzy, J.-R., Krause, S., Hannah, D. M., Fleckenstein, J. H., et al. (2015). Upscaling Nitrogen Removal Capacity from Local Hotspots to Low Stream Orders' Drainage Basins. *Ecosystems*, *18*(6), 1101–1120. https://doi.org/10.1007/s10021-015-9878-5

Poblador, S., Lupon, A., Sabaté, S., & Sabater, F. (2017). Soil water content drives spatiotemporal patterns of CO_2 and N_2O emissions from a Mediterranean riparian forest soil. *Biogeosciences*, *14*(18), 4195–4208. https://doi.org/10.5194/bg-14-4195-2017

Porporato, A., D'Odorico, P., Laio, F., & Rodriguez-Iturbe, I. (2003). Hydrologic Controls on Soil Carbon and Nitrogen Cycles. I. Modeling Scheme. *Advances in Water Resources*, *26*, 45–58. https://doi.org/10.1016/S0309-1708(02)00094-5

Pörtner, H.-O., Roberts, D. C., Tignor, M. M. B., Poloczanska, E. S., Mintenbeck, K., Alegría, A., et al. (Eds.). (2022). *Climate Change 2022: Impacts, Adaptation and Vulnerability.*

Contribution of Working Group II to the Sixth Assessment Report of the Intergovernmental Panel on Climate Change.

Ren, J., Adam, J. C., Hicke, J. A., Hanan, E. J., Tague, C. L., Liu, M., et al. (2021). How does water yield respond to mountain pine beetle infestation in a semiarid forest? *Hydrology and Earth System Sciences*, *25*(9), 4681–4699. https://doi.org/10.5194/hess-25-4681-2021

Ren, J., Hanan, E. J., Abatzoglou, J. T., Kolden, C. A., Tague, C. (Naomi) L., Kennedy, M. C., et al. (2022). Projecting Future Fire Regimes in a Semiarid Watershed of the Inland Northwestern United States: Interactions Among Climate Change, Vegetation Productivity, and Fuel Dynamics. *Earth's Future*, *10*(3), e2021EF002518. https://doi.org/10.1029/2021EF002518

Ren, J., Hanan, E., Greene, A. C., Tague, C., Krichels, A., Burk, W., et al. (2023). *Simulating the role of biogeochemical hotspots in driving nitrogen export from dryland watersheds* (preprint). Preprints. https://doi.org/10.22541/essoar.169168922.25673935/v1

Reyes, J. J., Tague, C. L., Evans, R. D., & Adam, J. C. (2017). Assessing the Impact of Parameter Uncertainty on Modeling Grass Biomass Using a Hybrid Carbon Allocation Strategy: A HYBRID CARBON ALLOCATION STRATEGY. *Journal of Advances in Modeling Earth Systems*, *9*(8), 2968–2992. https://doi.org/10.1002/2017MS001022

Rodriguez-Iturbe, I., Porporato, A., Ridolfi, L., Isham, V., & Coxi, D. R. (1999). Probabilistic modelling of water balance at a point: the role of climate, soil and vegetation. *Proceedings of the Royal Society of London. Series A: Mathematical, Physical and Engineering Sciences*, *455*(1990), 3789–3805. https://doi.org/10.1098/rspa.1999.0477

Rudgers, J. A., Luketich, A., Bacigalupa, M., Baur, L. E., Collins, S. L., Hall, K. M., et al. (2023). Infrastructure to factorially manipulate the mean and variance of precipitation in the field. *Ecosphere*, *14*(7), e4603. https://doi.org/10.1002/ecs2.4603

Ryan, M. G. (1991). Effects of Climate Change on Plant Respiration. *Ecological Applications*, *1*(2), 157–167. https://doi.org/10.2307/1941808

Ryan, T. M. (1991). *Soil Survey of Angeles National Forest Area, California* (p. Vol. 588-137). Glendora, CA.

Stephens, C. M., Marshall, L. A., Johnson, F. M., Lin, L., Band, L. E., & Ajami, H. (2020). Is Past Variability a Suitable Proxy for Future Change? A Virtual Catchment Experiment. *Water Resources Research*, *56*(2), e2019WR026275. https://doi.org/10.1029/2019WR026275

Stephens, C. M., Marshall, L. A., Johnson, F. M., Ajami, H., Lin, L., & Band, L. E. (2022). Spatial Variation in Catchment Response to Climate Change Depends on Lateral Moisture Transport and Nutrient Dynamics. *Water Resources Research*, *58*(10), e2021WR030577. https://doi.org/10.1029/2021WR030577

Sutton, M. A., Nemitz, E., Erisman, J. W., Beier, C., Bahl, K. B., Cellier, P., et al. (2007). Challenges in quantifying biosphere-atmosphere exchange of nitrogen species. *Environmental Pollution*, *150*(1), 125–139. https://doi.org/10.1016/j.envpol.2007.04.014

Tague, C. L., & Band, L. E. (2004). RHESSys: Regional Hydro-Ecologic Simulation System—An Object-Oriented Approach to Spatially Distributed Modeling of Carbon, Water, and Nutrient Cycling. *Earth Interactions*, *8*(19), 1–42. https://doi.org/10.1175/1087-3562(2004)8<1:RRHSSO>2.0.CO;2

Trenberth, K. E., Dai, A., Rasmussen, R. M., & Parsons, D. B. (2003). The Changing Character of Precipitation. *Bulletin of the American Meteorological Society*, *84*(9), 1205–1218. https://doi.org/10.1175/BAMS-84-9-1205

Welter, J. R., Fisher, S. G., & Grimm, N. B. (2005). Nitrogen Transport and Retention in an Arid Land Watershed: Influence of Storm Characteristics on Terrestrial–aquatic Linkages. *Biogeochemistry*, *76*(3), 421–440. https://doi.org/10.1007/s10533-005-6997-7

Winter, C., Nguyen, T. V., Musolff, A., Lutz, S. R., Rode, M., Kumar, R., & Fleckenstein, J. H. (2023). Droughts can reduce the nitrogen retention capacity of catchments. *Hydrology and Earth System Sciences*, *27*(1), 303–318. https://doi.org/10.5194/hess-27-303-2023

Wu, Q., Yue, K., Ma, Y., Heděnec, P., Cai, Y., Chen, J., et al. (2022). Contrasting effects of altered precipitation regimes on soil nitrogen cycling at the global scale. *Global Change Biology*, *28*(22), 6679–6695. https://doi.org/10.1111/gcb.16392

Ye, L., & Grimm, N. B. (2013). Modelling potential impacts of climate change on water and nitrate export from a mid-sized, semiarid watershed in the US Southwest. *Climatic Change*, *120*(1), 419–431. https://doi.org/10.1007/s10584-013-0827-z

Yu, Q., Duan, L., Yu, L., Chen, X., Si, G., Ke, P., et al. (2018). Threshold and multiple indicators for nitrogen saturation in subtropical forests. *Environmental Pollution*, *241*, 664–673. https://doi.org/10.1016/j.envpol.2018.06.001

Zhu, Q., Castellano, M. J., & Yang, G. (2018). Coupling soil water processes and the nitrogen cycle across spatial scales: Potentials, bottlenecks and solutions. *Earth-Science Reviews*, *187*, 248–258. https://doi.org/10.1016/j.earscirev.2018.10.005

Figure 1.

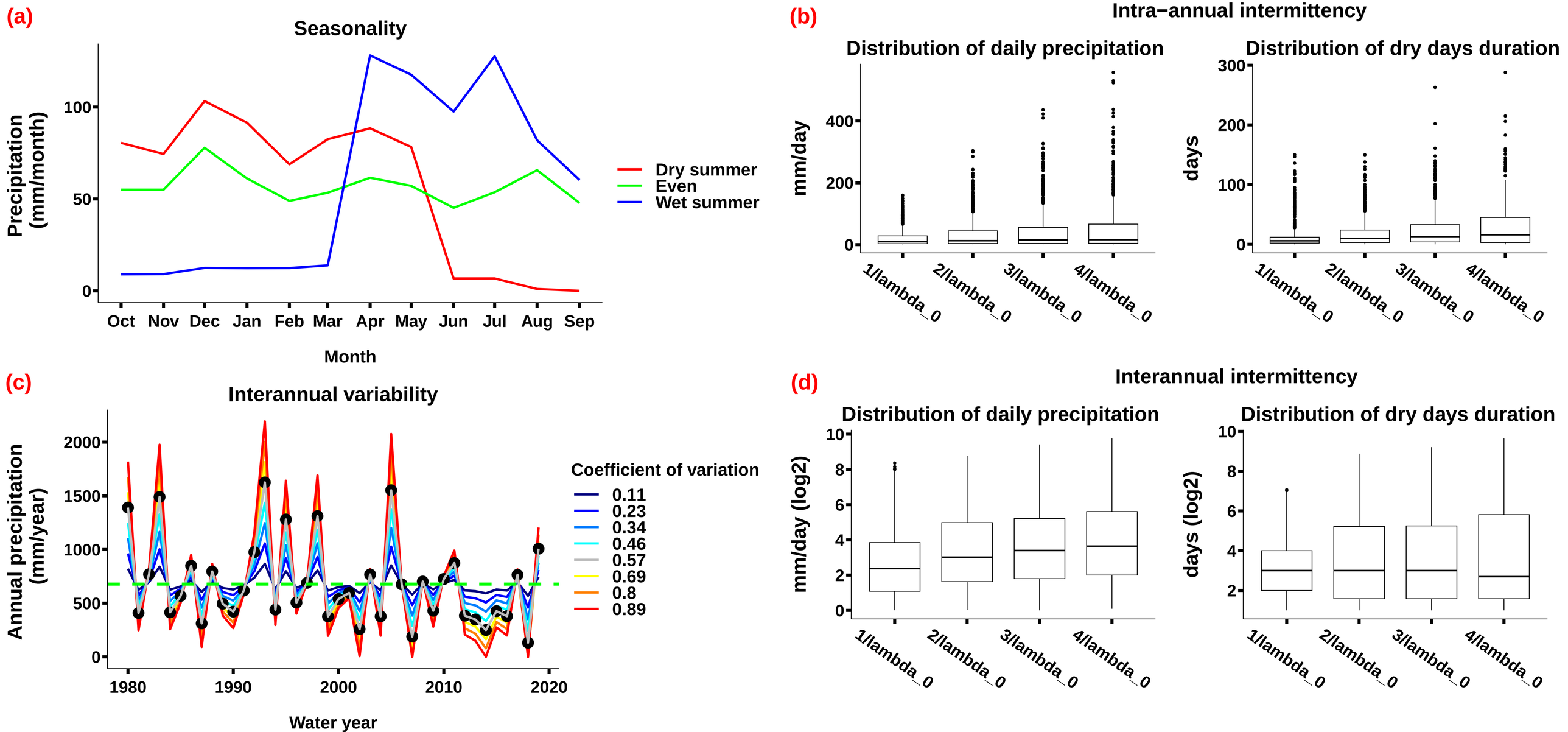
(a)
Seasonality
Precipitation (mm/month)
100
50
0
Oct Nov Dec Jan Feb Mar Apr May Jun Jul Aug Sep
Month
Dry summer
Even
Wet summer
(b)
Intra−annual intermittency
Distribution of daily precipitation
mm/day
400
200
0
1/lambda_0
2/lambda_0
3/lambda_0
4/lambda_0
Distribution of dry days duration
days
300
200
100
0
1/lambda_0
2/lambda_0
3/lambda_0
4/lambda_0
(c)
Interannual variability
Annual precipitation (mm/year)
2000
1500
1000
500
0
1980 1990 2000 2010 2020
Water year
Coefficient of variation
0.11
0.23
0.34
0.46
0.57
0.69
0.8
0.89
(d)
Interannual intermittency
Distribution of daily precipitation
mm/day (log2)
10
8
6
4
2
0
1/lambda_0
2/lambda_0
3/lambda_0
4/lambda_0
Distribution of dry days duration
days (log2)
10
8
6
4
2
1/lambda_0
2/lambda_0
3/lambda_0
4/lambda_0

Figure 2.

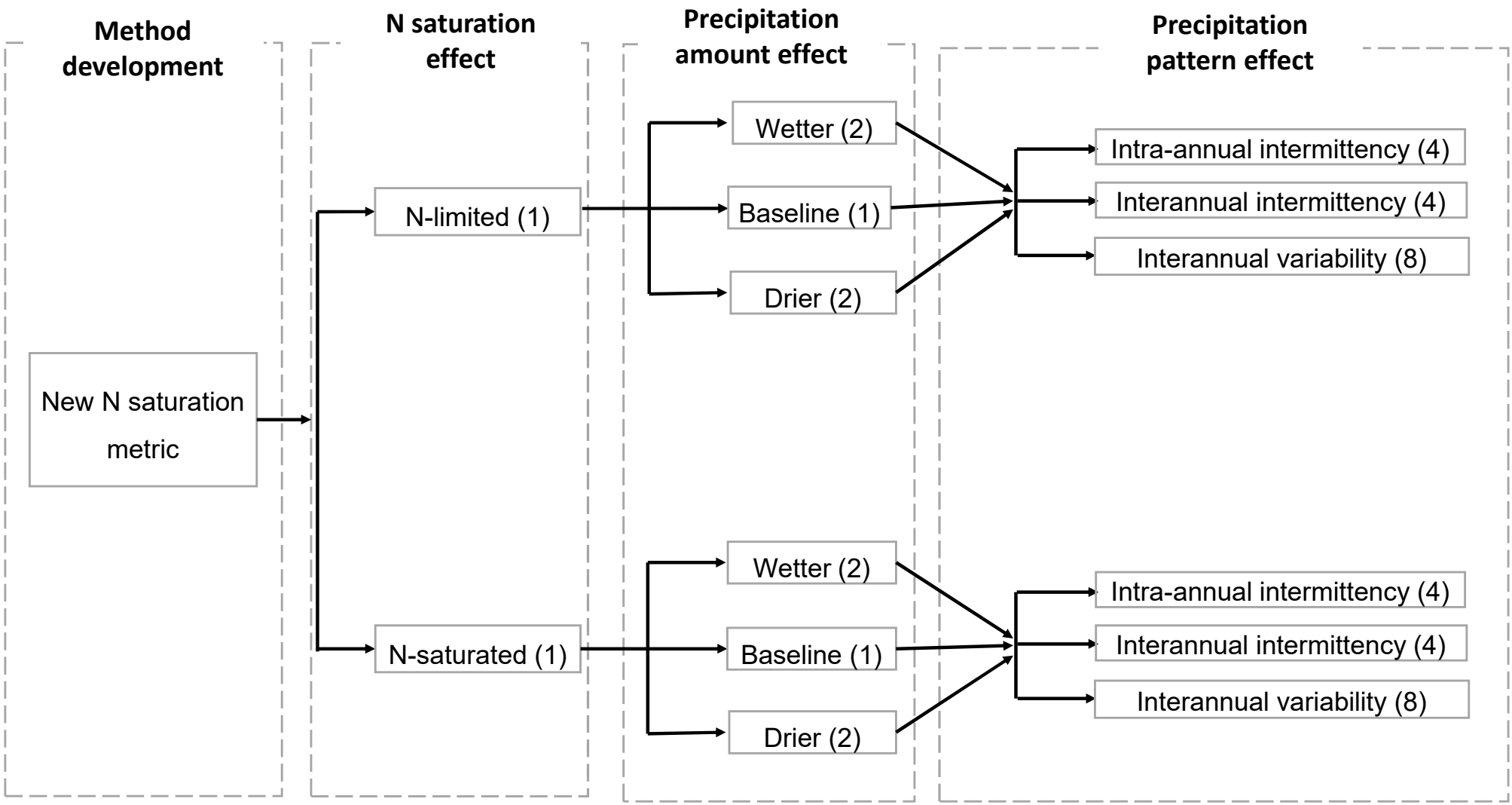
Method development
N saturation effect
Precipitation amount effect
Precipitation pattern effect
New N saturation metric
N-limited (1)
N-saturated (1)
Wetter (2)
Baseline (1)
Drier (2)
Wetter (2)
Baseline (1)
Drier (2)
Intra-annual intermittency (4)
Interannual intermittency (4)
Interannual variability (8)
Intra-annual intermittency (4)
Interannual intermittency (4)
Interannual variability (8)

Figure 3.

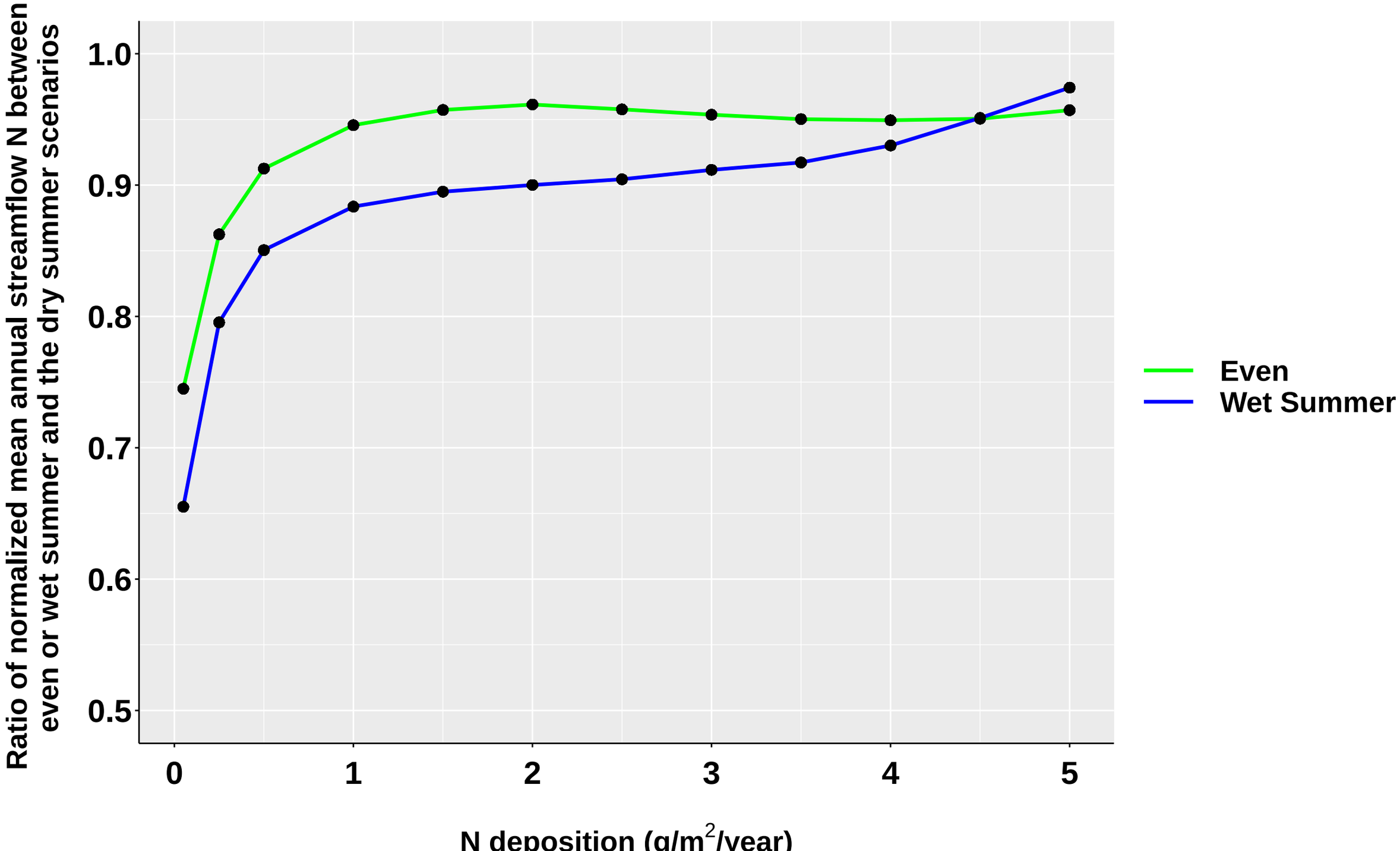
Ratio of normalized mean annual streamflow N between even or wet summer and the dry summer scenarios
1.0
0.9
0.8
0.7
0.6
0.5
0
1
2
3
4
5
N deposition (g/m2/year)
Even
Wet Summer

Figure 4.

N−saturated

(a)

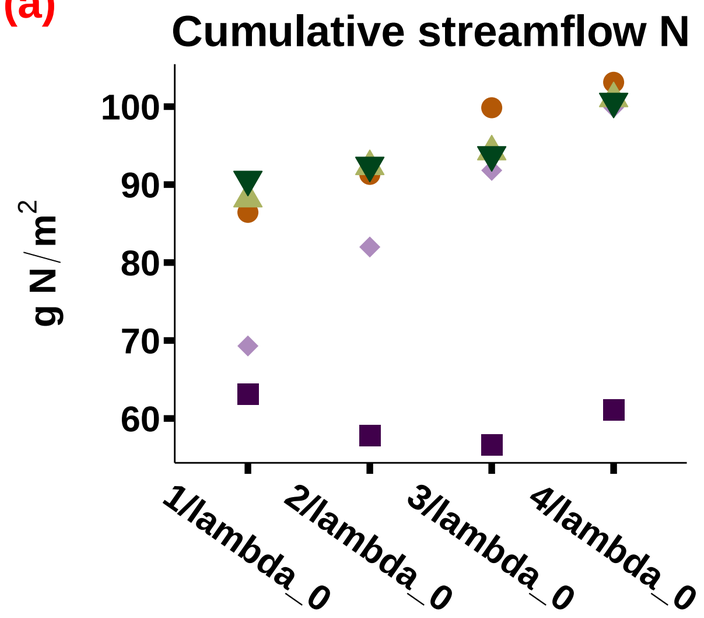

(b)

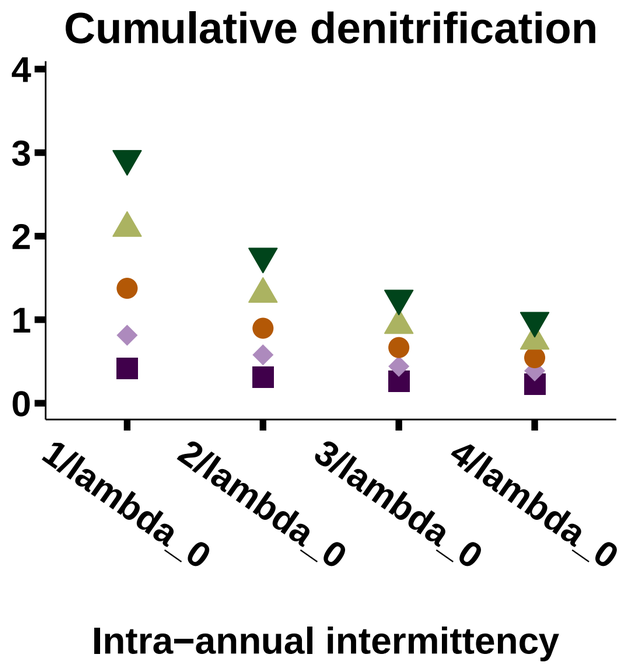

(c)

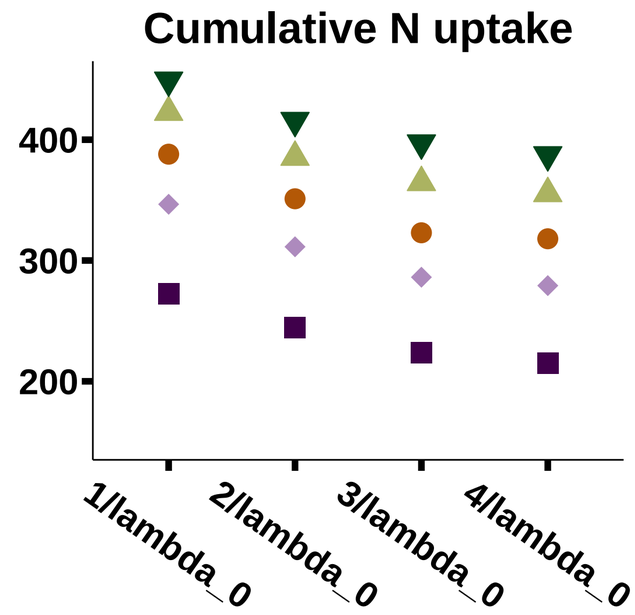

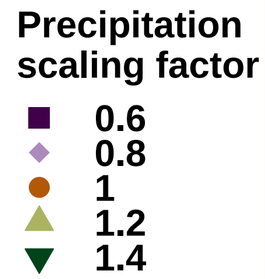

N−limited

(d)

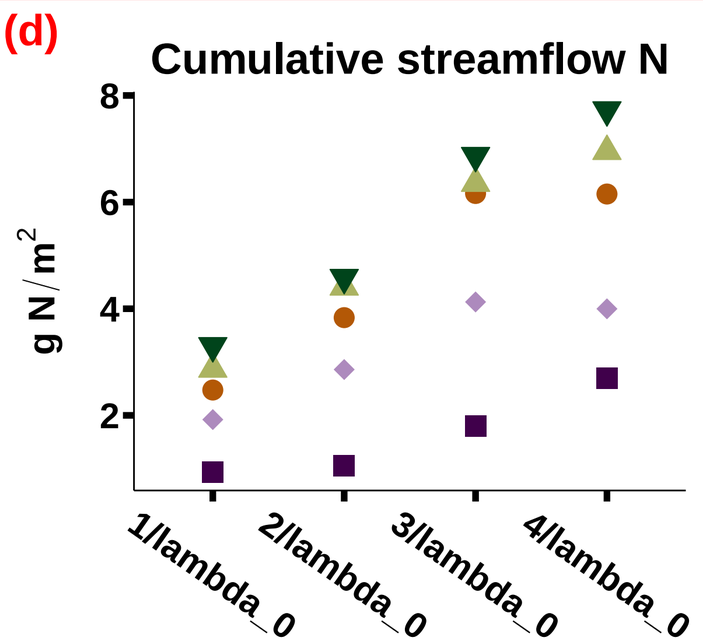

(e)

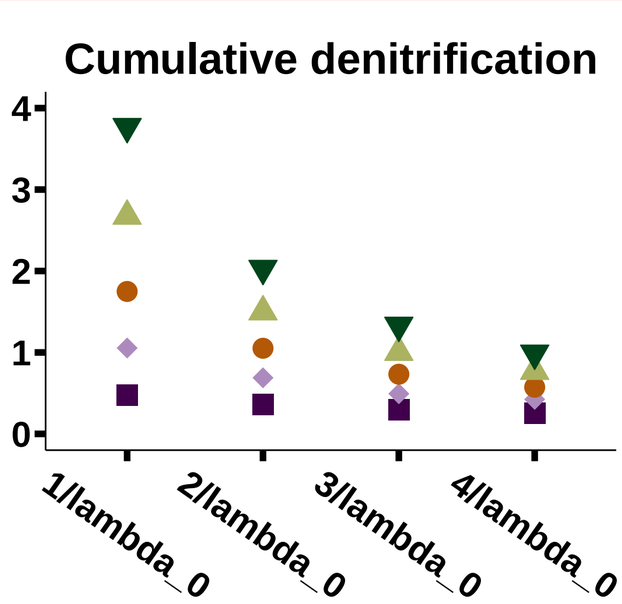

(f)

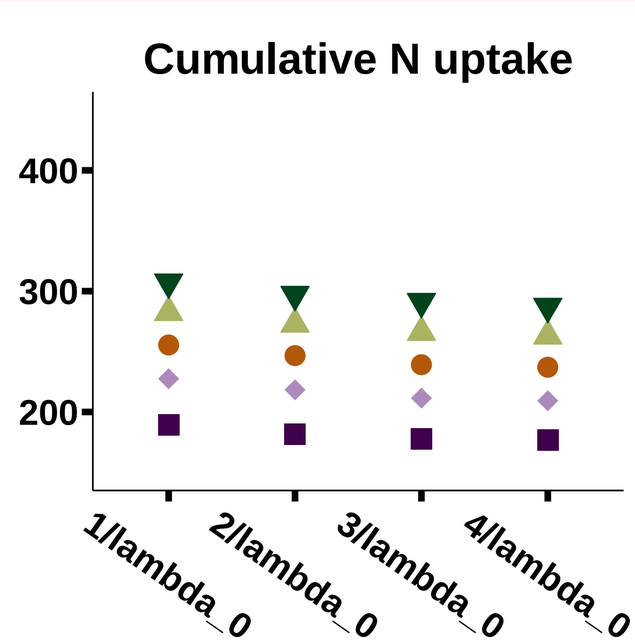

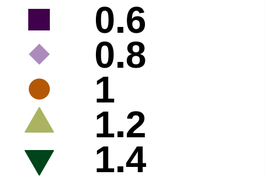

Figure 5.

N−saturated

(a)

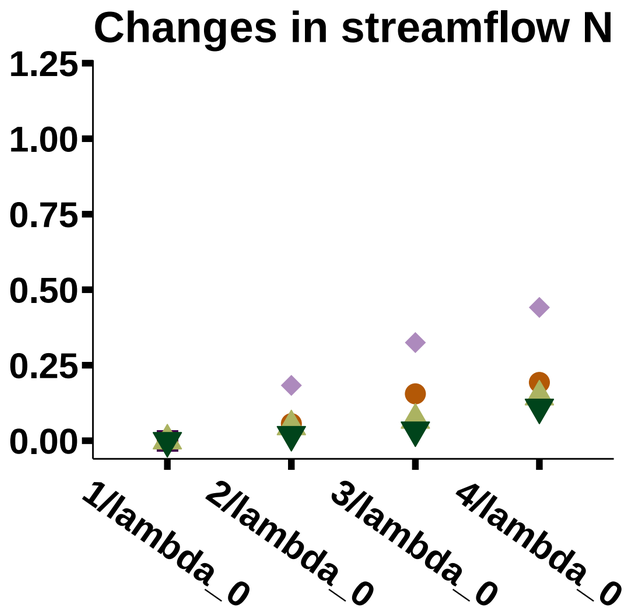

(b)

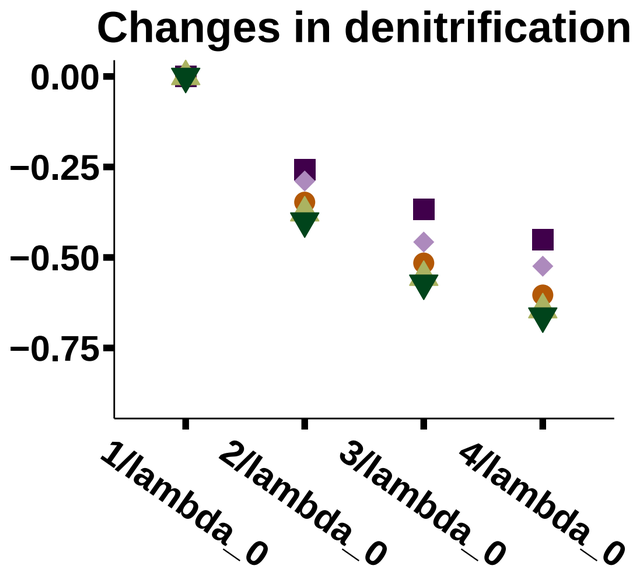

(c)

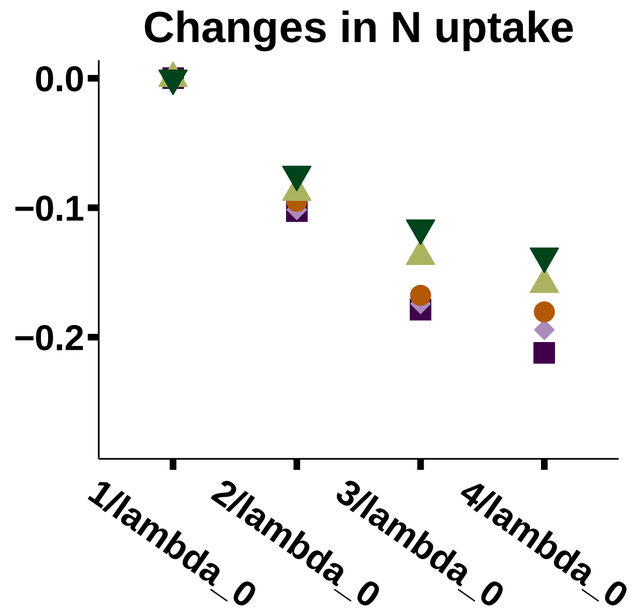

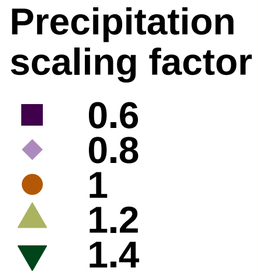

N−limited

(d)

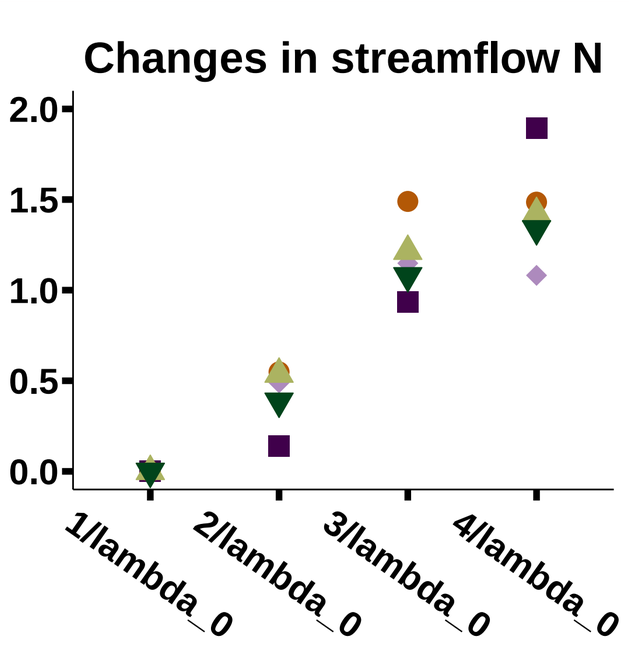

(e)

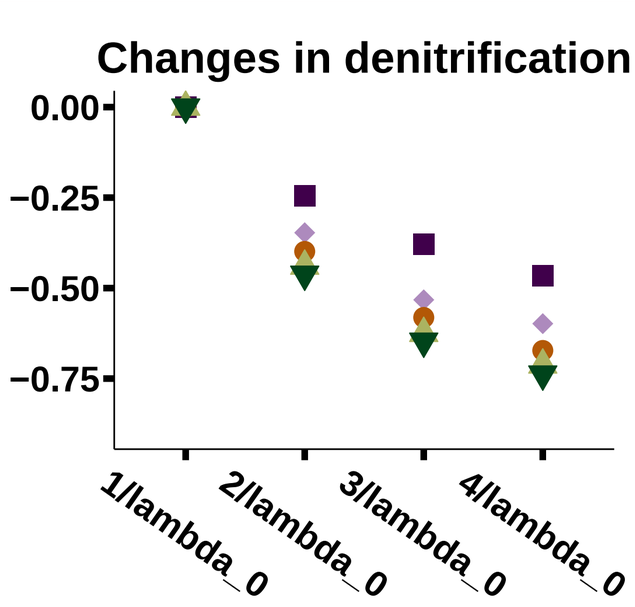

(f)

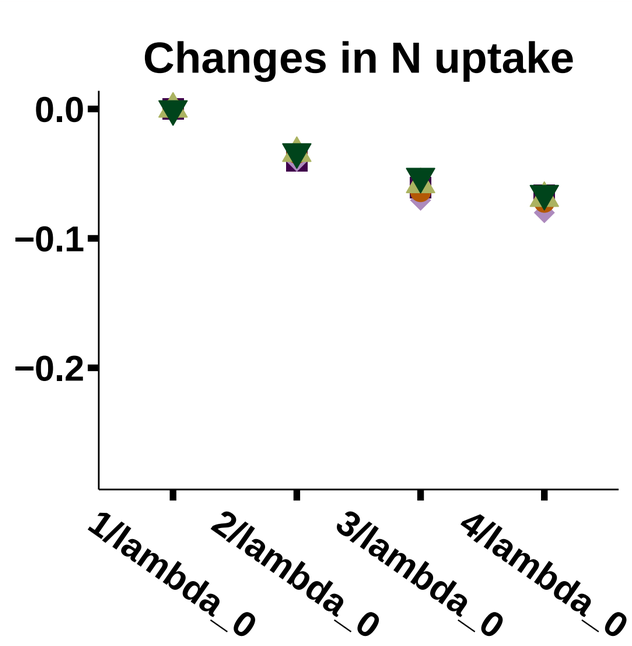

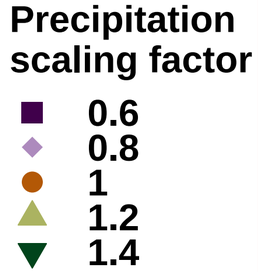

Figure 6.

N−saturated

(a)

Cumulative streamflow N

g N / m^2

200
100
0

1/lambda_0
2/lambda_0
3/lambda_0
4/lambda_0

(b)

Cumulative denitrification

20
15
10
5
0

1/lambda_0
2/lambda_0
3/lambda_0
4/lambda_0

Interannual intermittency

(c)

Cumulative N uptake

500
400
300
200
100

1/lambda_0
2/lambda_0
3/lambda_0
4/lambda_0

Precipitation scaling factor
0.6
0.8
1
1.2
1.4

N−limited

(d)

Cumulative streamflow N

g N / m^2

200
100
0

1/lambda_0
2/lambda_0
3/lambda_0
4/lambda_0

(e)

Cumulative denitrification

20
15
10
5
0

1/lambda_0
2/lambda_0
3/lambda_0
4/lambda_0

Interannual intermittency

(f)

Cumulative N uptake

500
400
300
200
100

1/lambda_0
2/lambda_0
3/lambda_0
4/lambda_0

Precipitation scaling factor
0.6
0.8
1
1.2
1.4

Figure 7.

N−saturated

(a)

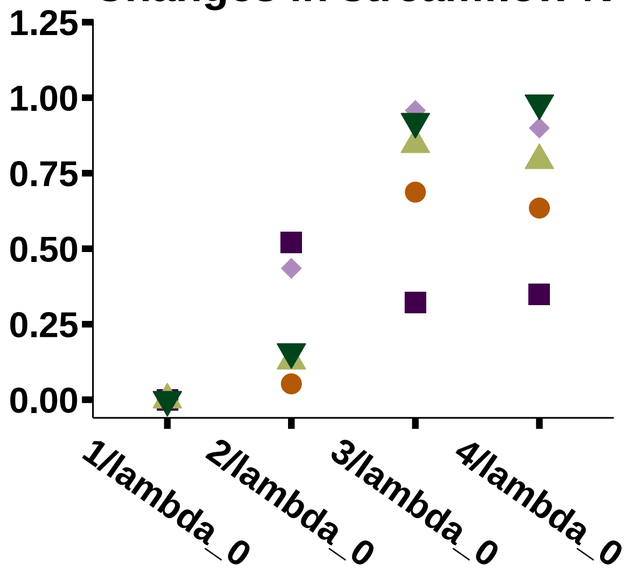

(b)

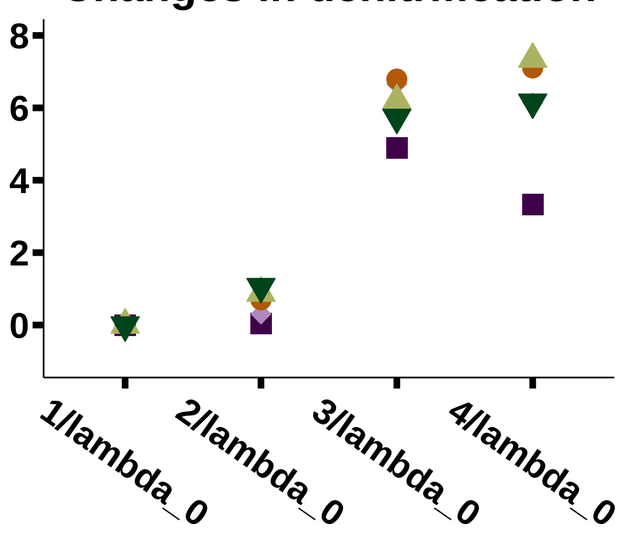

(c)

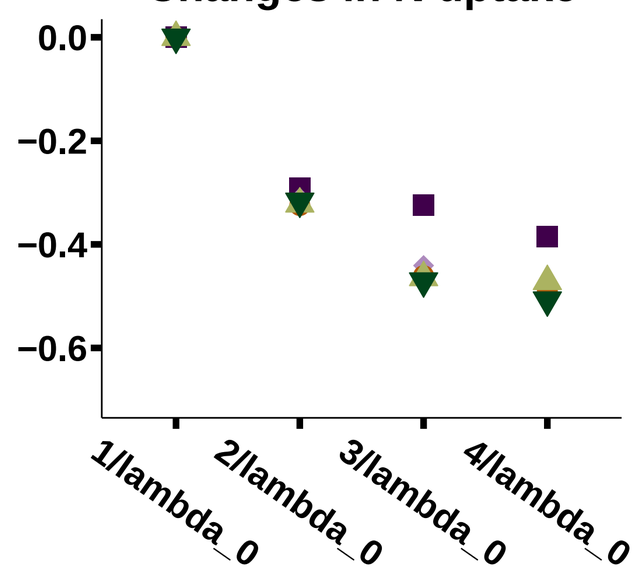

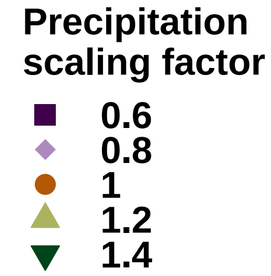

N−limited

(d)

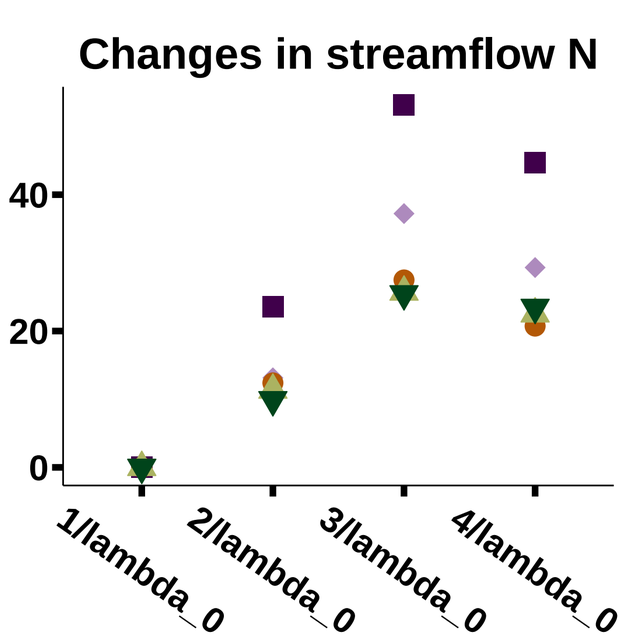

(e)

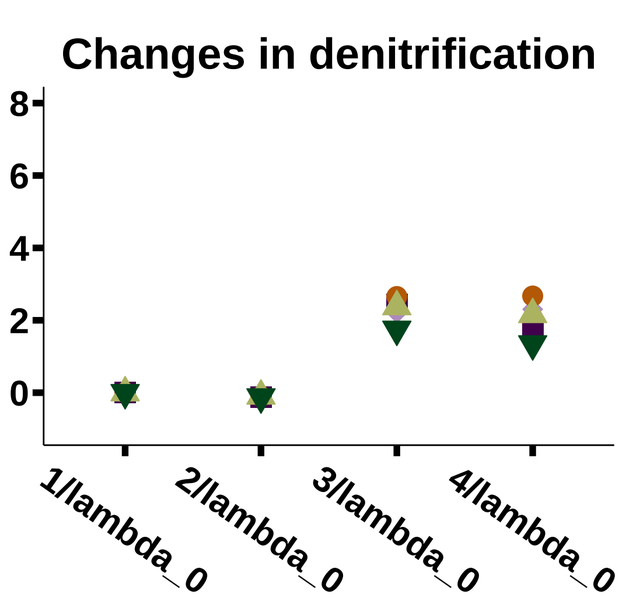

(f)

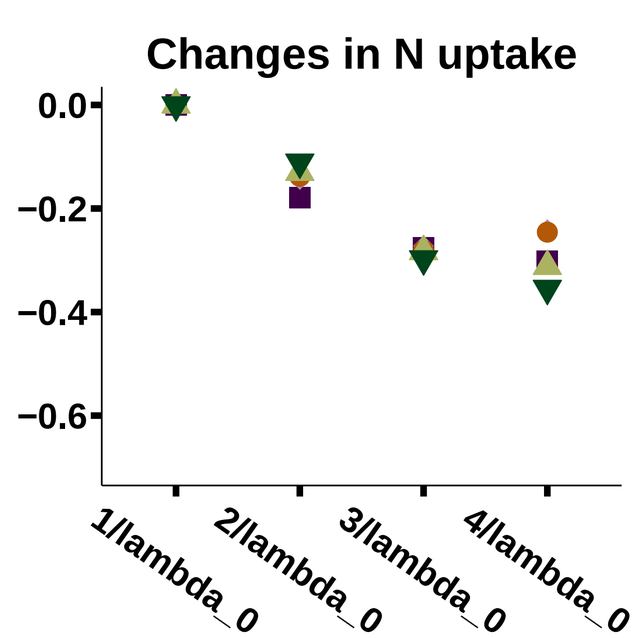

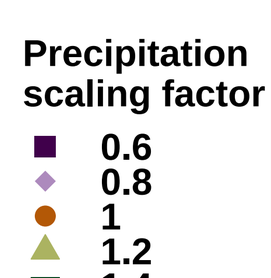

Figure 8.

N−saturated

(a)

Cumulative streamflow N

g N / m^2

175
150
125
100
75

0.11 0.23 0.34 0.46 0.57 0.69 0.8 0.89

(b)

Cumulative denitrification

6
4
2
0

0.11 0.23 0.34 0.46 0.57 0.69 0.8 0.89

CV of annual precipitation

(c)

Cumulative N uptake

400
300
200

0.11 0.23 0.34 0.46 0.57 0.69 0.8 0.89

Precipitation scaling factor
0.6
0.8
1
1.2
1.4

N−limited

(d)

Cumulative streamflow N

g N / m^2

15
10
5

0.11 0.23 0.34 0.46 0.57 0.69 0.8 0.89

(e)

Cumulative denitrification

6
4
2
0

0.11 0.23 0.34 0.46 0.57 0.69 0.8 0.89

CV of annual precipitation

(f)

Cumulative N uptake

400
300
200

0.11 0.23 0.34 0.46 0.57 0.69 0.8 0.89

Precipitation scaling factor
0.6
0.8
1
1.2
1.4

Figure 9.

N−saturated

(a)

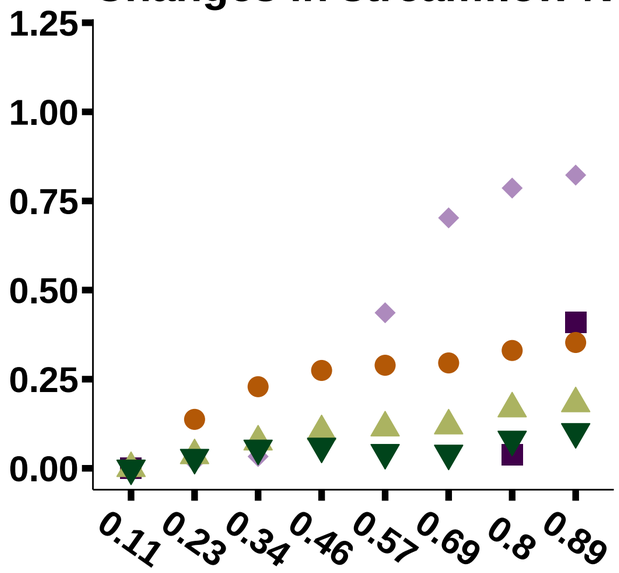

(b)

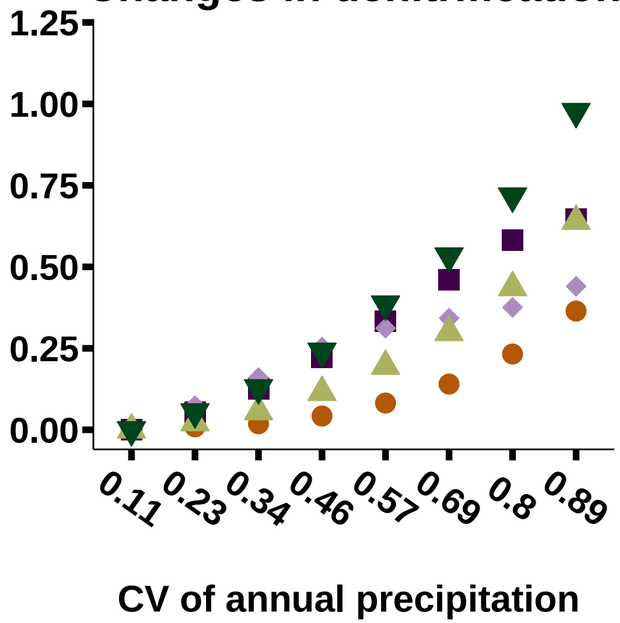

(c)

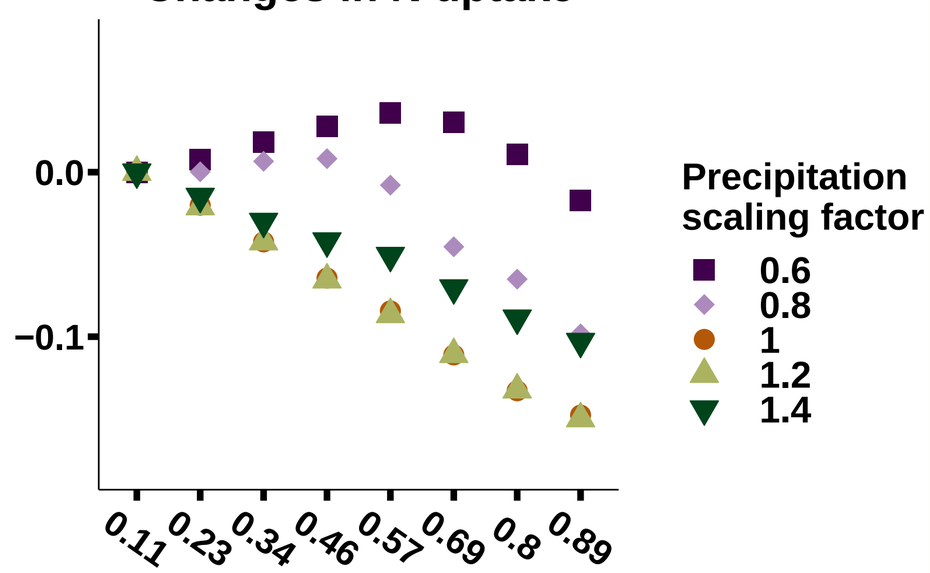

N−limited

(d)

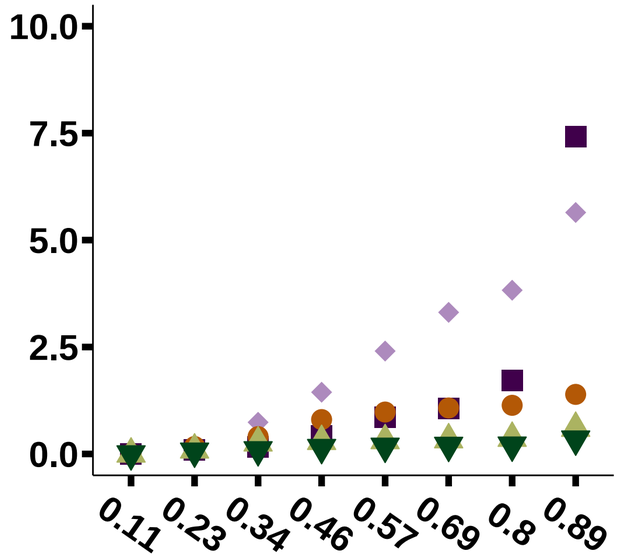

(e)

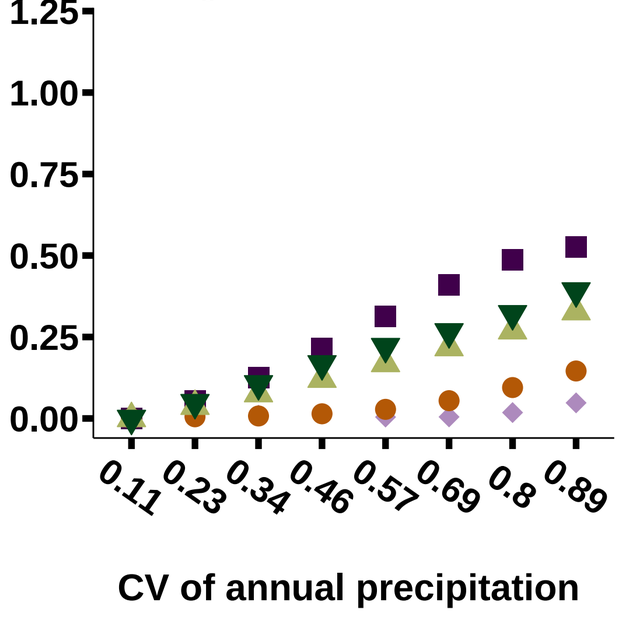

(f)

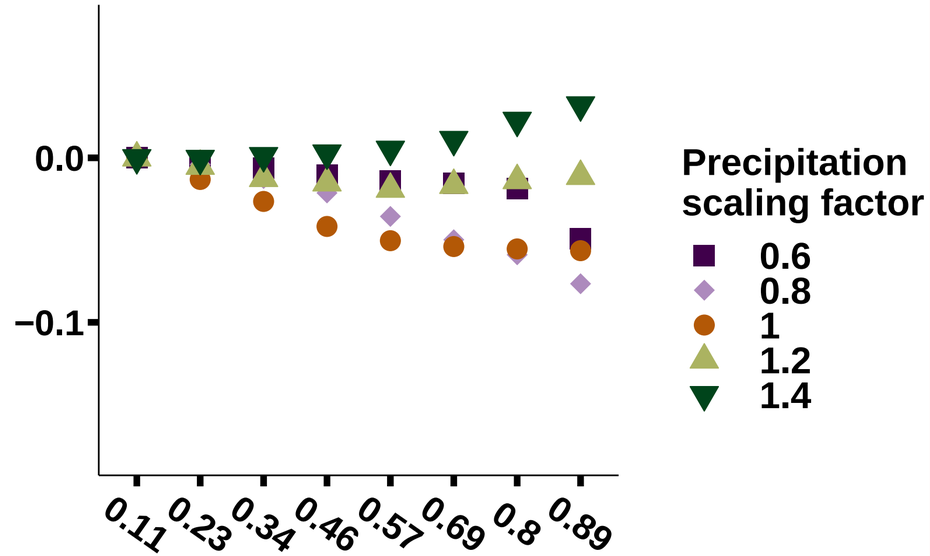

Figure 10.

N−saturated

(a) Intra−annual intermittency

(b) Interannual intermittency

(c) Interannual variability

Ratio (Total N export/N deposition)

1.00
0.75
0.50
0.25
0.00

1/lambda_0
2/lambda_0
3/lambda_0
4/lambda_0

0.11
0.23
0.34
0.46
0.57
0.69
0.8
0.89

Precipitation regime changes

Precipitation scaling factor
0.6
0.8
1
1.2
1.4

N−limited

(d) Intra−annual intermittency

(e) Interannual intermittency

(f) Interannual variability

Ratio (Total N export/N deposition)

6
4
2
0

30
20
10
0

1/lambda_0
2/lambda_0
3/lambda_0
4/lambda_0

0.11
0.23
0.34
0.46
0.57
0.69
0.8
0.89

Precipitation regime changes

Precipitation scaling factor
0.6
0.8
1
1.2
1.4

Figure 11.

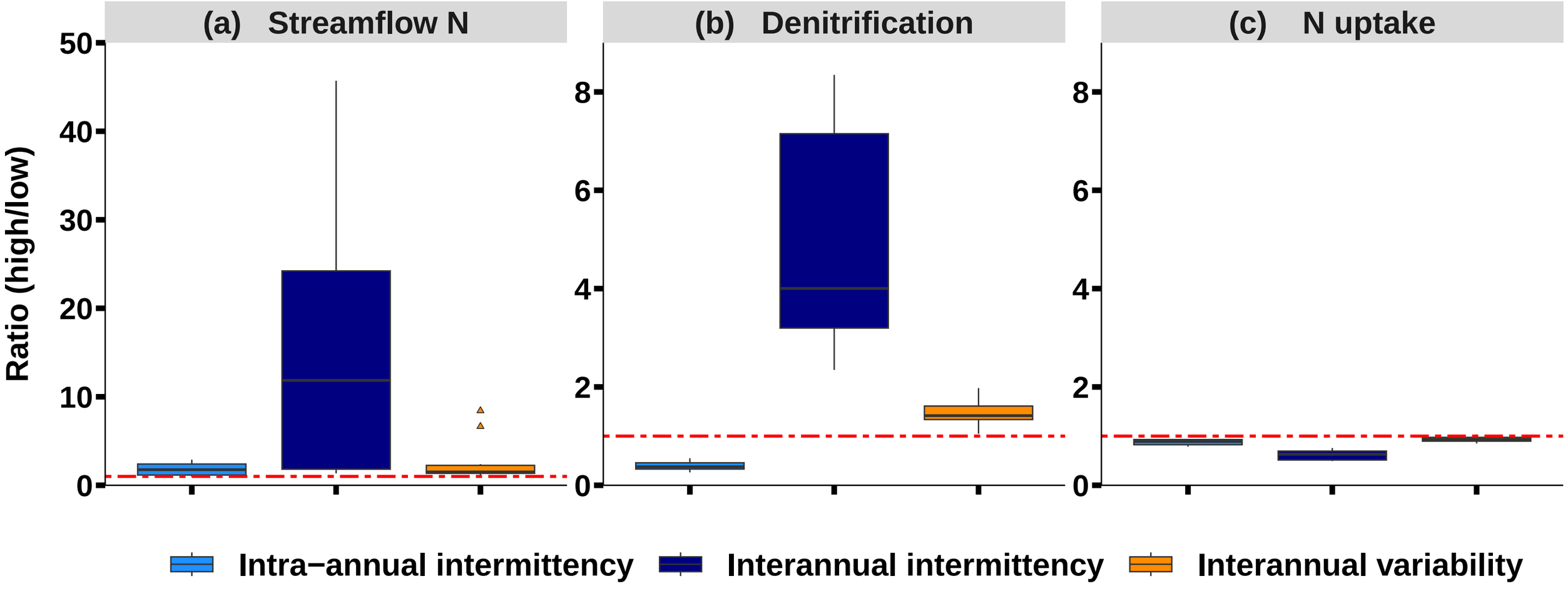
(a) Streamflow N
(b) Denitrification
(c) N uptake
Ratio (high/low)
50
40
30
20
10
0
8
6
4
2
0
Intra−annual intermittency
Interannual intermittency
Interannual variability

Figure 12.

(a) Streamflow N
(b) Denitrification
(c) N uptake
(d) Streamflow N
(e) Denitrification
(f) N uptake
(g) Streamflow N
(h) Denitrification
(i) N uptake
g N / m2
Ratio (wet/dry)
Ratio (N−saturated/N−limited)
0.6
0.8
1
1.2
1.4
Precipitation scaling factor
N−limited
N−saturated